RESEARCH ARTICLE

Key Points:
- Best documented TGF observed at ground
- Second TGF induced by triggered lightning
- An ICC pulse occurred simultaneously (within 20 μs) of the TGF

Correspondence to:
B. M. Hare,
hare@phys.ufl.edu

Ground-level observation of a terrestrial gamma ray flash initiated by a triggered lightning

B. M. Hare[1], M. A. Uman[2], J. R. Dwyer[3], D. M. Jordan[2], M. I. Biggerstaff[4], J. A. Caicedo[2], F. L. Carvalho[2], R. A. Wilkes[2], D. A. Kotovsky[2], W. R. Gamerota[2], J. T. Pilkey[2], T. K. Ngin[2], R. C. Moore[2], H. K. Rassoul[5], S. A. Cummer[6], J. E. Grove[7], A. Nag[8], D. P. Betten[4], and A. Bozarth[5]

[1]Department of Physics, University of Florida, Gainesville, Florida, USA, [2]Department of Electrical and Computer Engineering, University of Florida, Gainesville, Florida, USA, [3]Department of Physics and Space Science Center (EOS), University of New Hampshire, Durham, New Hampshire, USA, [4]School of Meteorology, University of Oklahoma, Norman, Oklahoma, USA, [5]Department of Physics, Florida Institute of Technology, Melbourne, Florida, USA, [6]Electrical and Computer Engineering, Duke University, Durham, North Carolina, USA, [7]Naval Research Laboratory, Washington, District of Columbia, USA, [8]Vaisala Inc, Louisville, Colorado, USA

Abstract We report on a terrestrial gamma ray flash (TGF) that occurred on 15 August 2014 coincident with an altitude-triggered lightning at the International Center for Lightning Research and Testing (ICLRT) in North Central Florida. The TGF was observed by a ground-level network of gamma ray, close electric field, distant magnetic field, Lightning Mapping Array (LMA), optical, and radar measurements. Simultaneous gamma ray and LMA data indicate that the upward positive leader of the triggered lightning flash induced relativistic runaway electron avalanches when the leader tip was at about 3.5 km altitude, resulting in the observed TGF. Channel luminosity and electric field data show that there was an initial continuous current (ICC) pulse in the lightning channel to ground during the time of the TGF. Modeling of the observed ICC pulse electric fields measured at close range (100–200 m) indicates that the ICC pulse current had both a slow and fast component (full widths at half maximum of 235 μs and 59 μs) and that the fast component was more or less coincident with the TGF, suggesting a physical association between the relativistic runaway electron avalanches and the ICC pulse observed at ground. Our ICC pulse model reproduces moderately well the measured close electric fields at the ICLRT as well as three independent magnetic field measurements made about 250 km away. Radar and LMA data suggest that there was negative charge near the region in which the TGF was initiated.

1. Introduction

Terrestrial gamma ray flashes (TGFs) are intense bursts of gamma radiation with durations from tens to hundreds of microseconds that originate within thunderstorms and are commonly detected on Earth-orbiting satellites. TGFs were originally detected by the Burst and Transient Source Experiment (BATSE) on the Compton Gamma Ray Observatory (CGRO) [*Fishman et al.*, 1994]. TGFs have since been observed by other experiments on the Reuven Ramaty High Energy Solar Spectroscopic Imager (RHESSI), Fermi, and Astro-Rivelatore Gamma a Immagini Leggero (AGILE) satellites [e.g., *Smith et al.*, 2005; *Briggs et al.*, 2010; *Marisaldi et al.*, 2010]. TGFs can be so intense that they cause satellite instruments that were designed to observe solar X-ray and gamma ray emissions to experience severe instrumental saturation [e.g., *Grefenstette et al.*, 2008; *Briggs et al.*, 2011; *Marisaldi et al.*, 2010]. Furthermore, TGFs potentially pose a significant health hazard for individuals in aircraft flying near thunderstorms [*Dwyer et al.*, 2010]. Analysis of RHESSI and Fermi TGF data indicate that most TGFs originate within thunderstorms below 15 km altitude [e.g., *Dwyer and Smith*, 2005; *Cummer et al.*, 2005; *Lu et al.*, 2010; *Shao et al.*, 2010; *Østgaard et al.*, 2013; *Cummer et al.*, 2014, 2015].

Two TGFs have previously been detected at ground level at the International Center for Lightning Research and Testing (ICLRT), a 1 km[2] facility located five miles east of Starke, FL, in North Central Florida. One TGF was associated with a 2003 classically triggered lightning flash [*Dwyer et al.*, 2004a], and the other followed a return stroke in a natural cloud-to-ground flash in 2009 [*Dwyer et al.*, 2012]. A third ground-level TGF was detected by the Lightning Observatory in Gainesville, FL, in 2015 [*Tran et al.*, 2015]. Here we report on a fourth TGF, one that was associated with an altitude-triggered flash at the ICLRT on 15 August 2014. The 2014 TGF is by far the best documented of any ground-observed TGF. The 2014 TGF shared a number of common features with the 2003 TGF, as we will discuss.

Another phenomenon related to TGFs and observed on the ground is the thunderstorm "gamma ray glow" [e.g., *McCarthy and Parks*, 1985; *Chilingarian et al.*, 2010]. However, gamma ray glows are fundamentally distinct from TGFs, since gamma ray glows occur on time scales of seconds to tens of minutes, while TGFs occur on time scales of tens to hundreds of microseconds. Furthermore, TGFs are observed in correlation with lightning flashes, particularly intracloud flashes raising negative charge [e.g., *Inan et al.*, 1996; *Cummer et al.*, 2005; *Shao et al.*, 2010; *Cohen et al.*, 2010; *Connaughton et al.*, 2010; *Lu et al.*, 2010; *Cummer et al.*, 2011; *Østgaard et al.*, 2013; *Cummer et al.*, 2014, 2015], and *Dwyer* [2012] have provided modeling that shows how TGFs could be directly initiated by lightning flashes, whereas glows are not correlated with lightning flashes and tend to be terminated by lightning flashes [*McCarthy and Parks*, 1985]. *Chilingarian et al.* [2010] refer to all thunderstorm gamma ray flux detected at ground level as thunderstorm ground enhancements, regardless of the duration of the gamma ray flux. In this paper we follow the precedent set by *Dwyer et al.* [2004a, 2012] and *Tran et al.* [2015] that thunderstorm gamma ray fluxes with durations on the order of tens to hundreds of microseconds, even if they are detected at ground level, are referred to as TGFs.

At the ICLRT, lightning is artificially initiated (triggered) from natural thunderstorms by elevating a grounded triggering wire toward the thunderstorms with a rocket, so-called rocket- and wire-triggered lightning [e.g., *Rakov and Uman*, 2003]. Once the rocket and wire reach about 300 m altitude, an upward moving positively charged leader (UPL) may propagate from the grounded-wire tip toward the thunderstorm seeking regions of negative charge and initiating a classically triggered lightning flash. Occasionally, whether by accident or on purpose, the triggering wire will become disconnected from ground and the triggering process will create an altitude-triggered lightning flash [e.g., *Lalande et al.*, 1998; *Rakov and Uman*, 2003]. The altitude-triggered flash is different from the more common classically triggered flash in that in the former the triggering wire is not grounded, resulting in a downward stepped negative leader propagating from the bottom of the wire a few milliseconds after a UPL is initiated from its top. Once the downward negative stepped leader attaches to ground, it initiates a return stroke that travels up the negative leader, through the triggering wire, to the top of the UPL, where the return stroke terminates. After the return stroke stops, the UPL continues upward [e.g., *Lalande et al.*, 1998; *Rakov and Uman*, 2003; *Dwyer and Uman*, 2013]. In both altitude and classically triggered lightning, as the UPL travels toward and into the thunderstorm, the current at the base of the lightning channel transitions from the UPL current to the initial continuous current (ICC), which is a relatively steady current on the order of hundreds of Amperes. *Pilkey et al.* [2014] suggest that the transition from UPL current to ICC occurs when the UPL reaches and propagates into a negative charge region, a transition generally associated with the observation of channel branching. The UPL and ICC together are referred to as the initial stage (IS) of the triggered lightning. There can be impulsive variations in the channel current during the IS. These are called ICC pulses.

In this paper we primarily show and analyze data collected from the 2014 TGF. First, in section 2, we review pertinent features of the 2003 TGF. In section 3 we discuss the 2014 TGF and the altitude-triggered lightning flash that initiated it. Figure 1 contains a map of the ICLRT showing the locations of most of the measurements to be discussed in section 3. In section 3.1 we present high-energy scintillator data associated with the TGF. In sections 3.2 and 3.3 we give electric field data and high-speed camera data to demonstrate that there was an ICC pulse coincident with the TGF. Sections 3.4, 3.5, and 3.6 present Lightning Mapping Array (LMA) data, quasi-static electric field data, and radar data in order to identify the location of the TGF and to help infer the cloud-charge distribution before and during the TGF. In section 3.7 we show distant magnetic field data, which have been used in previous studies to characterize TGFs [e.g., *Inan et al.*, 1996; *Cummer et al.*, 2005; *Lu et al.*, 2010; *Shao et al.*, 2010; *Cummer et al.*, 2011; *Connaughton et al.*, 2010, 2013; *Østgaard et al.*, 2013; *Cummer et al.*, 2014, 2015]. In section 4 we discuss two models that are used in analyzing the measured data. In section 5 we compare data from the 2003 TGF to the 2014 TGF, along with a further discussion of some of the 2014 data. Finally, in section 6, we summarize all results and present conclusions. A related theoretical paper is presently being written that will use all available data, including gamma ray data not included in the present paper, to model the 2014 TGF and associated high-energy processes.

2. The 2003 TGF

As noted above, a TGF was observed at ground level at the ICLRT during the initial stage of a grounded-wire (classical) rocket-triggered flash. The TGF occurred 40 ms after the initiation of the UPL [*Dwyer et al.*, 2004a]. *Dwyer et al.* [2004a] used this time, along with an average expected UPL speed, to estimate that the source of the TGF was between 6 and 8 km above ground. However, since it is now known that North Florida UPLs often
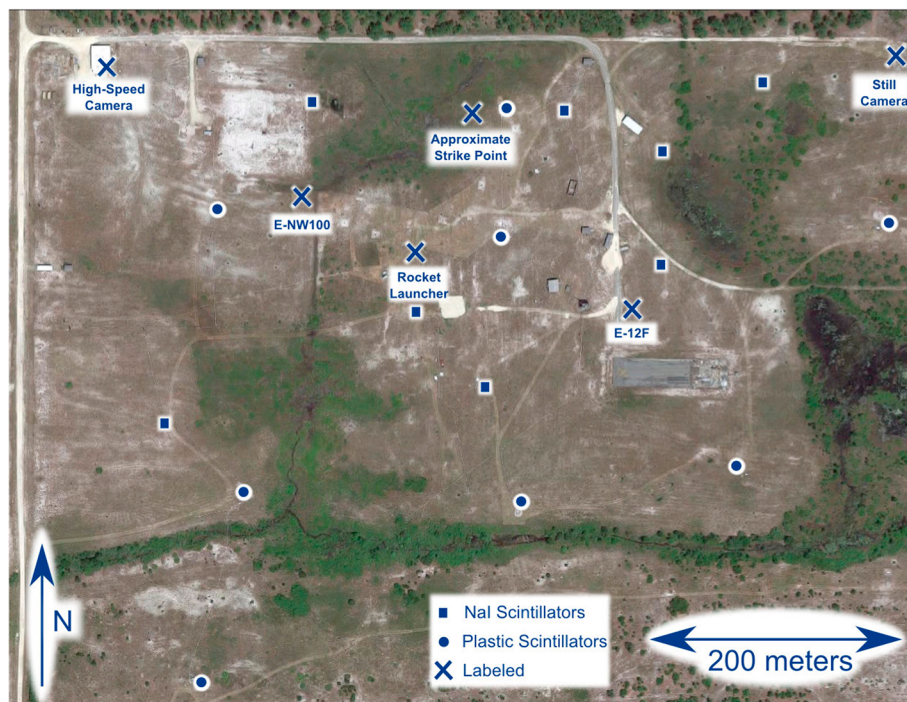
Figure 1. Map of the ICLRT with the 2014 altitude trigger strike point, the rocket launcher, and instrument locations associated with measurements in this paper identified. E-NW100 and E-12F are electric field antennas.

turn horizontal in regions of negative charge near the 0°C level [*Hill et al.*, 2012, 2013; *Pilkey et al.*, 2014], it is possible that the source of the TGF source was lower than 6 km. Figure 2 shows the measured ground-level gamma radiation and the channel-base current associated with the 2003 TGF. The gamma radiation from the TGF was about 250 µs in duration and was coincident with a large ICC pulse. The triggering of the 2003 gamma radiation measurement and the ground-based current were independent, so there could be some error in their alignment in Figure 2. From other measurements, we estimate that the detected gamma rays shown in Figure 2 could have occurred up to 30 µs after the time shown in Figure 2, but not before the time shown in Figure 2. This unidirectional timing error has only been discovered recently and was not known
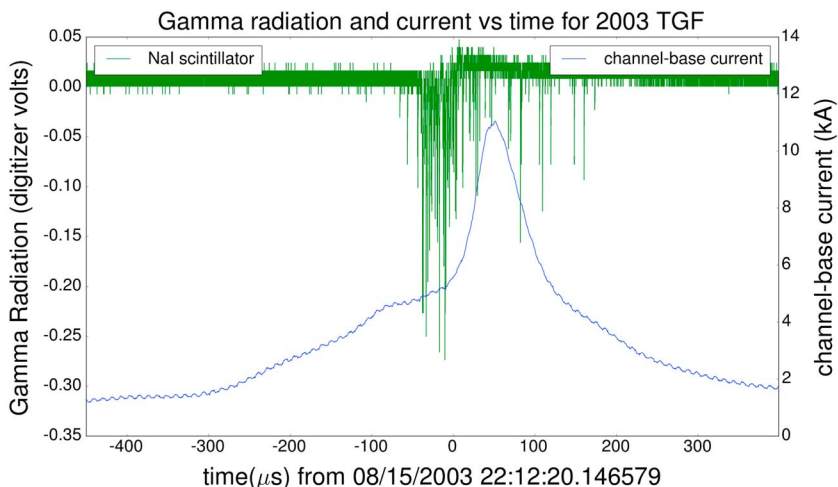
Figure 2. Gamma radiation and channel-base current during the 2003 TGF, where each downward going spike represents gamma rays detected by an unshielded NaI scintillator. The triggering of the 2003 gamma radiation measurement and the ground-based current were independent; thus, there could be some error in their alignment. We estimate from other measurements that the gamma rays could have occurred up to 30 µs after the time shown by the green trace in this figure but could not have occurred before the time shown.
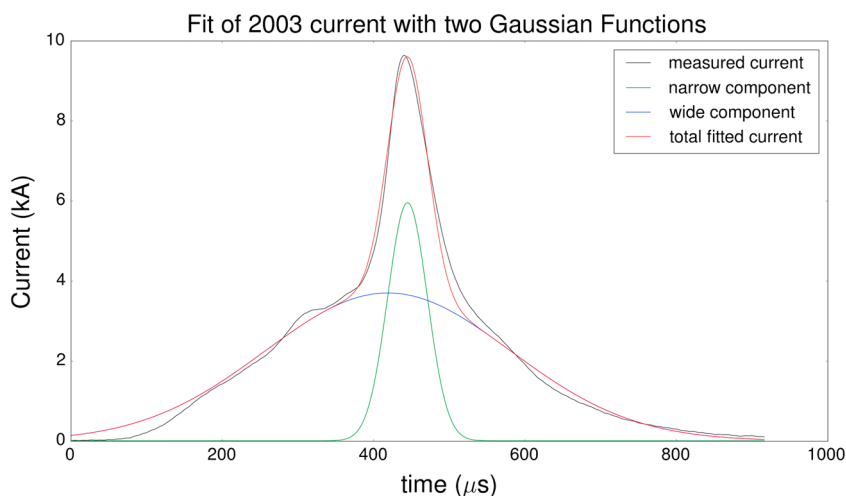
Figure 3. Two Gaussian functions are used to fit the measured channel-base current of the 2003 TGF. The two Gaussians have amplitudes of 3.7 kA and 5.9 kA and FWHMs of 765 μs and 59 μs, respectively. The 1.3 kA underlying steady current is not shown. Time 0 in this figure was chosen to match with time 0 in equation (1) and is 382 μs before the time 0 in Figure 2.

in *Dwyer et al.* [2004a]. However, the results and conclusions in *Dwyer et al.* [2004a] do not rely on the exact timing of this gamma ray measurement and so are unaffected by our discovery of the up to 30 μs timing error. The ICC pulse appears to be the sum of two Gaussian functions, as illustrated in Figure 3. Figure 3 shows the channel-base current, with the 1.3 kA steady ICC current removed, fit to a slowly varying and a more rapidly varying Gaussian with amplitudes of 3.7 kA and 5.9 kA and full widths at half maximum (FWHM) of 765 μs and 75 μs, respectively. Most ICC pulses are asymmetric and so are not Gaussian. We analyzed 56 ICC pulses and found that only nine of them could be well fit by a single Gaussian curve, and only one appeared to be composed of the combination of simultaneous slow and fast Gaussians. The fact that the measured ICC channel-base current for the 2003 TGF can be decomposed into two Gaussian functions is significant and
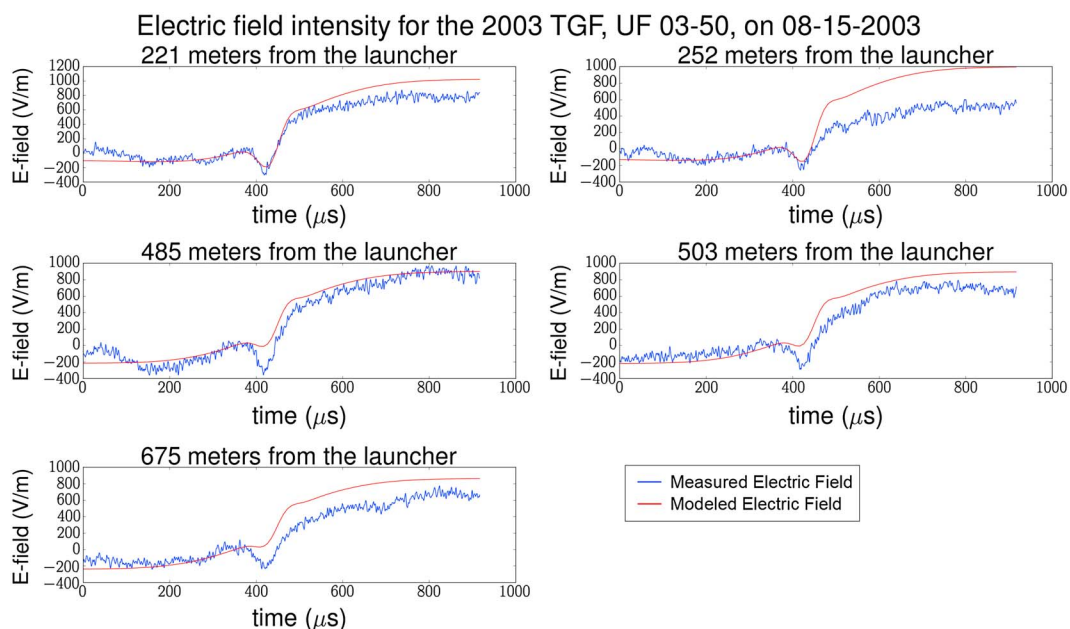
Figure 4. Measured (blue) and modeled (red) electric fields associated with the ICC pulse current during the 2003 TGF. Time 0 in this figure was chosen to match with time 0 in equation (1) and is 382 μs before the time 0 in Figure 2. This electric field was measured with flat-plate antennas that are not sensitive to the quasi-static electric field, so the zero level, DC offset, of the electric field in this figure is arbitrary. We have also adjusted the DC offset of the modeled fields in order to compare them to the measured electric fields.

appears also to be the case for the 2014 TGF, as discussed in section 5. Figure 4 shows close multiple-station electric fields measured at different distances from the rocket launcher, not previously published, associated with the ICC pulse, and it depicts modeled electric fields, which will be discussed in section 4 along with the modeled fields for the 2014 event.

3. Overview of the 2014 TGF

On 15 August 2014, two triggered lightning flashes were initiated 7 min apart. The first flash, designated UF 14-53, was a classically triggered flash containing five return strokes. We examine UF 14-53 (section 3.4) because it provides evidence of the atmospheric charge structure prior to the next triggered flash, UF 14-54, a rocket launch followed by an inadvertent altitude-triggered flash that was associated with the 2014 TGF. After the UF 14-54 rocket was launched, the grounded triggering wire broke so that the upward moving rocket trailed a segment of ungrounded wire. The ambient electric field was high enough to cause an upward positive leader (UPL) to initiate from the top of the wire and a negative stepped leader to initiate from the bottom of the wire. When the negative stepped leader attached to the ground, it initiated a return stroke that traveled up the leader channel, through the wire, to the top of the UPL where the return stroke terminated. The UPL then continued upward from that point toward the overhead negative charge. Figure 5 is a still-camera photograph with a 5 s exposure showing the wire segment, path of the negative stepped leader below the wire, and the path of the lower part of the upward positive leader above the wire. The wire segment is directly over the launcher, the strike point about 116 m NNE of the launcher. Figure 1 shows the approximate location of the downward negative leader attachment to the ground and the launcher location. Since the flash did not strike the rocket launcher, we were not able to directly measure the channel-base current, but we will use a model, in section 4, to estimate the channel-base current magnitude and wave shape from the measured close electric field and distant magnetic field data. During this altitude-triggered flash, electric field data were recorded by two close electric field sensors. Both antenna systems had an upper frequency cutoff around 20 MHz, limited by the fiber optics carrying the signal to the recording oscilloscope. One electric field sensor, labeled E-12F (Figure 1), was a circular flat metallic plate flush with the ground and insulated from the ground, located 180 m southeast of the rocket launcher and 200 m southeast of the strike point. The associated electronics provided a system decay time constant to a step function input field of 1.23 s. The other antenna, labeled E-NW100 (Figure 1), was an elevated inverted-bowl type with a decay time constant of 7.8 s. It was located 108 m northwest of the launcher and 150 m southwest from the strike point. Since these electric field antennas are not sensitive to the quasi-static electric field, the zero level is arbitrary and only the change in electric field is meaningful. Figure 6 shows about 20 ms of the electric field from E-12F: the initial electric field change due to the downward negative leader and upward positive leader, the field change from the return stroke and upward positive leader, the field change from just the upward positive leader following the return stroke's termination at the then-height of the UPL, and the field change from the ICC pulse associated with the TGF.

A second leader-return stroke sequence, not shown in Figure 6, occurred 324 ms after the first return stroke. This second leader-return stroke sequence was not associated with a UPL so was not expected to produce a TGF. It could have produced dart leader X-rays, which is the case with many dart leaders, but probably did not since none of the X-ray or gamma ray measurements recorded signals during the second leader/return stroke sequence.

Thirteen milliseconds after the first, truncated, return stroke, a relatively large ICC pulse occurred in the lightning channel, and the ICLRT gamma ray network (see section 3.1) and ground-based detectors operated by the Naval Research Lab (NRL) detected a TGF of about 290 μs duration. The ICLRT-measured duration of the TGF was taken to be the time between the first gamma ray detected by any of the ICLRT plastic scintillators and the last gamma ray detected by any of the ICLRT plastic scintillators. The TGF duration could certainly have been longer than 290 μs, since there could have been gamma rays from the TGF outside of our start and stop times that were not detected by any of the ICLRT scintillators.

The National Lightning Detection Network (NLDN) detected three impulsive events associated with this flash; a −7.4 kA misidentified intracloud flash, coincident in time with the electromagnetic fields of the first truncated return stroke of the altitude-triggered flash, a 14.2 kA intracloud flash, which was due to the electromagnetic fields of the ICC pulse and the TGF currents, and a −10.9 kA cloud-to-ground return stroke associated with the second, and final, return stroke of the triggered flash.
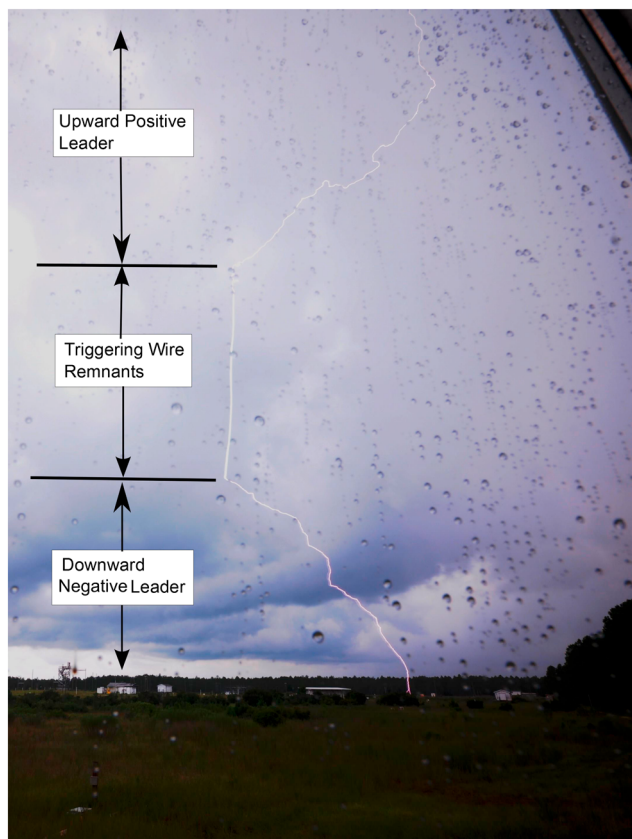
Figure 5. Photograph of UF 14-54, taken looking west, shows the path of the downward negative leader, the wire remnants, and the path of the bottom of the upward positive leader. The top of the triggering wire remnants was 286 m above the ground, and the triggering wire remnants were 134 m long. The part of the upward positive leader seen here developed at about the same time (likely initiated milliseconds before) as the downward negative leader, before the first, truncated, return stroke. The wire segment is directly above the launcher. Locations are shown in Figure 1. The photograph is a 5 s time exposure that has been contrast enhanced.

The 2014 TGF was detected with a specially designed TGF trigger circuit in use since the summer of 2014. Signals from eight shielded NaI scintillators are fed into this trigger circuit. When the output level exceeds a certain threshold, a network of oscilloscopes recording a subset of the TERA data (section 3.1) is triggered and data are recorded for 1 s. The threshold level is set so that the trigger circuit does not respond to background noise but will trigger on both X-rays bursts from lightning leaders, which generally have microsecond duration and occur periodically, and signals from the high energy radiation from in-cloud-initiated TGFs, which have durations on the order of 100 μs. The data are then examined to separate the signals of lightning leaders from potential TGFs. The TGF trigger circuit detected the 2014 TGF at 17:04:18.517714 UTC, which was just after the start of the TGF, as shown in Figure 7. In addition to the TGF trigger circuit installed in 2014, X-ray and gamma ray measurements are triggered and recorded when all of the instruments at the ICLRT are triggered, which is either by the luminosity of on-site natural lightning strokes or by the triggered lightning stroke current. Hence, all X-ray and gamma ray measurements are recorded whenever there is a full system trigger, but since summer 2014, TGFs can be detected without a full system trigger in the event that they are not directly associated with cloud-to-ground natural lightning or triggered lightning.

To supplement the information given here, a related paper is presently being written to address the TGF photon measurements by the separate detection facility operated by the Naval Research Lab at the ICLRT, along with modeling of the TGF that takes into account all of the available measurements.

3.1. TERA Data
High-energy photon data from the 2014 TGF were collected by a subset of the ICLRTs Thunderstorm Energetic Radiation Array (TERA) [*Dwyer et al.*, 2012]. This subset includes eight unshielded 7.6 cm × 7.6 cm cylindrical NaI scintillators, eight 7.6 cm × 7.6 cm cylindrical NaI scintillators shielded by 0.32 cm thick lead, eight 1 m²,
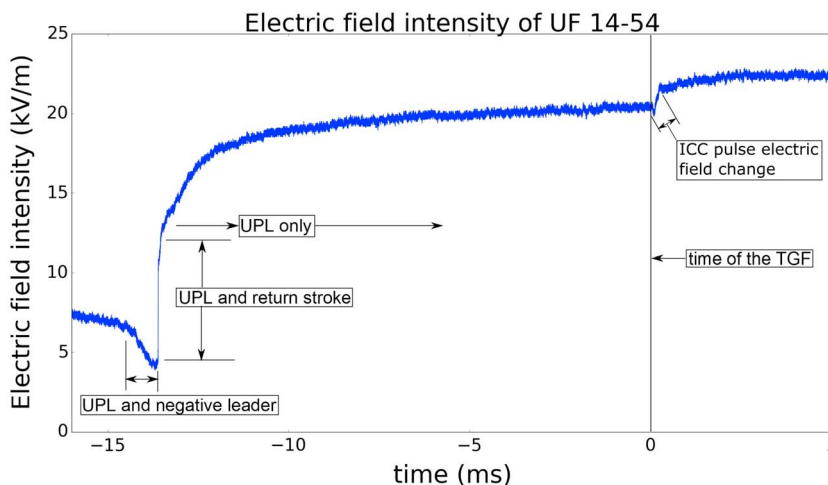
Figure 6. Electric field intensity recorded during UF 14-54 measured by E-12F 185 m from the rocket launcher and 200 m from the ground strike point (see Figure 1) shows the electric field change due to the upward positive leader (UPL) and the downward negative leader, the upward positive leader and the return stroke, and then just the upward positive leader. Since the UPL likely initiated a few milliseconds before the downward negative leader and continued as the return stroke traversed it, the electric field measured during the downward negative leader and the return stroke contains components due to the upward positive leader as well. The TGF occurred at $t = 0$. This electric field was measured with a flat-plate antennas that are not sensitive to the quasi-static electric field, so the zero level, DC offset, of the electric field in this figure is arbitrary.

2 cm thick, organic plastic scintillators, and a single 7.6 cm × 7.6 cm cylindrical LaBr$_3$ scintillator. Each of these instruments was housed inside a 0.32 cm thick aluminum box in order to shield the scintillators from RF noise. The data from these scintillators were transmitted over optical fiber cables to a central location where they were digitized and stored on digital oscilloscopes. These instruments experience two different modes of saturation. Most commonly, the optical transmitters used to send the data over fiber optic cabling saturate when the output signal is between ±1.0 V and ±1.5 V. Less commonly, the photomultiplier tubes (PMTs) attached to the scintillators can saturate in special conditions.

Figure 7 shows data collected from an unshielded NaI scintillator during the time of the TGF. The red and green bars indicate the approximate start and stop times of the TGF found, as noted earlier, by locating the first and
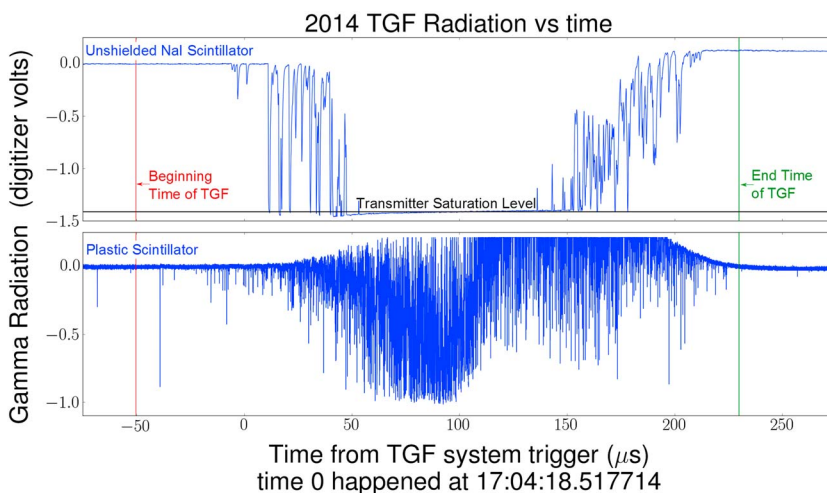
Figure 7. Data recorded by an unshielded NaI scintillator and a plastic scintillator during the 2014 terrestrial gamma ray flash. Each downward spike represents gamma radiation being detected by the scintillators. The gamma flux was so high that pileup occurred so that by 50 µs after the system trigger the electronics completely saturated. The red and green vertical bars show the beginning and end of the TGF, respectively, these times being found from data from the plastic scintillators.
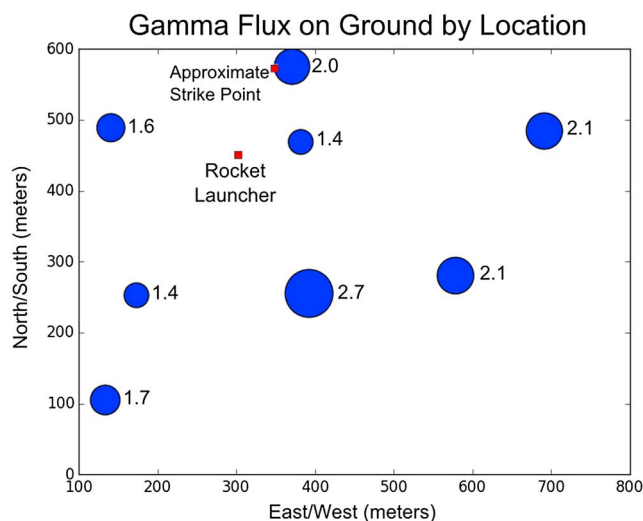
Figure 8. Relative count flux of the TGF on the ground versus location during a 47.8 μs period prior to the saturation of any detector. Each blue circle represents a plastic scintillator, where the radius of the circle is proportional to the flux received by that detector. The red square indicates the location of the rocket launcher used to trigger the lightning flash. This measured flux value for each detector is next to the appropriate circle in units of counts per square meter per microsecond.

last gamma rays detected by any of the plastic scintillators. It is clear that the TGF had an extremely high peak flux, large enough that pulse pileup caused all of the scintillators to experience significant saturation of the optical transmitters. Some of the scintillators, such as the unshielded NaI scintillator used in Figure 7, experienced such severe optical transmitter saturation that the detectors remained saturated for over 100 μs. None of the NaI scintillators showed evidence that their PMTs were saturated, but it is entirely possible that their PMTs did saturate at the same time that their optical transmitters were saturated. All of the plastic scintillators, such as the one whose data are shown in Figure 7, show evidence that both their PMTs and optical transmitter were saturated. The LaBr$_3$ scintillator's PMT saturated without the optical transmitter saturating. While it is not possible to produce a meaningful spectrogram from the data collected from the ICLRT scintillators, there were a number of multi-MeV photons detected before the scintillators saturated.

The count rate due to background radiation was measured for the unshielded NaI scintillator over a period of 800 ms directly after the TGF and was found to be about 136 counts per second. Thus, very few, if any, of the counts shown in Figure 7 for the unshielded NaI scintillator are due to background radiation.

Note that these scintillator signals could not have been due to radio frequency electromagnetic interference from the lightning, since the ICLRT high-energy network is very well shielded from lightning radio frequency electromagnetic interference, and even during return strokes from very close lightning flashes, there are no false signals. Furthermore, the pulses shown in Figure 7 have the exact shape expected from gamma radiation.

Figure 8 shows the spatial distribution of count flux across the ICLRT for the early portion of the records (prior to saturation) of the plastic scintillators shown in Figure 1. Each blue circle is the location of a 1 m^2 plastic scintillator, and the size of the circle indicates the average flux received by that detector during a 47.8 μs time period before any of the detectors began to saturate. The approximate value for the flux is written next to each blue circle in units of counts per square meter per microsecond. Because each detector potentially has a different noise level and different photomultiplier power supply voltage, the flux values can only be compared to each other with a risk of considerable error. There does not appear to be any clear spatial distribution of the TGF flux on the ground. However, Figure 8 does show that the TGF beam spanned at least our entire array which is about 500 m by 500 m.

3.2. ICC Pulse Electric Fields
Figure 9 gives the two close (105 m, 185 m from the launcher and 150 m, 200 m, from the ground strike point) electric field measurements recorded during the time of the 2014 TGF. Figure 9 also shows the modeled electric field using an ICC pulse model that is described in section 4, the same model used to describe the
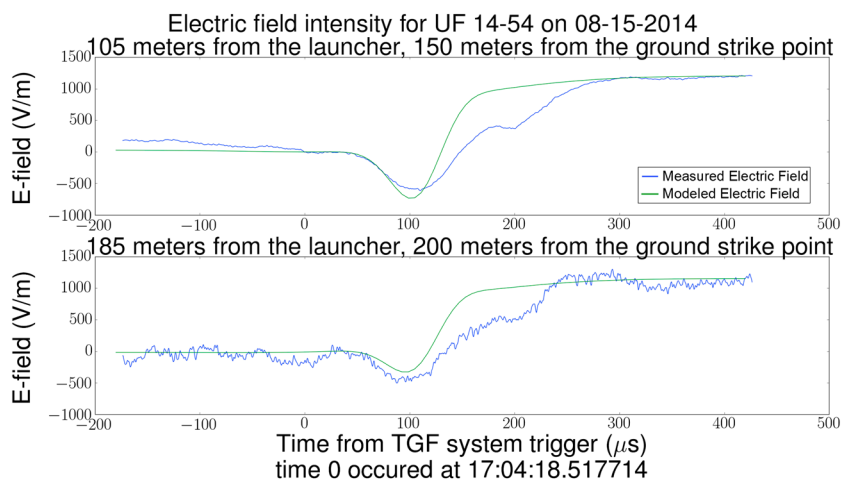
Figure 9. The 2014 TGF electric field measured (blue) at two different locations and modeled (green) as a perfectly vertical channel above the rocket launcher. This electric field was measured with flat-plate antennas that are not sensitive to the quasi-static electric field, so the zero level, DC offset, of the electric field in this figure is arbitrary. We have also adjusted the DC offset of the modeled fields in order to compare them to the measured electric fields.

close fields of the 2003 TGF shown in Figure 4. The electric fields in Figures 4 and 9 are not dissimilar from those of a typical ICC pulse.

3.3. High-Speed Video

A Phantom V73 high-speed camera, operated 280 m from the rocket launcher (see Figure 1) with an average frame rate of 6.5 kfps, recorded the channel of the altitude-triggered lightning associated with the 2014 TGF. Figure 10 shows six high-speed video frames during the time of the 2014 TGF. The numbers above each frame indicate the UTC time stamp associated with the beginning of each frame. Figure 11 shows the integrated channel luminosity of these frames superimposed on the recorded electric field from antenna E-NW100 at 105 m from the launcher (Figure 1). Together, these figures verify that there was a brightening in the lightning channel which, along with the data in Figure 9, verifies that there was an ICC pulse during the time of the TGF.

3.4. Lightning Mapping Array

The eight station VHF lightning mapping array (LMA) at the ICLRT is used to track the breakdown sources at the front of propagating leader channels such as the triggered lightning's upward propagating positive leader (UPL). The ICLRT LMA is described in detail by *Pilkey et al.* [2014] and *Pilkey* [2014]. Each LMA station records the amplitude and time of VHF pulse emissions (68–72 MHz) in 10 μs intervals, with the largest impulse in that interval being tagged and potentially located in 3-D. The timing uncertainty of the ICLRT LMA has been estimated to be 30–40 ns [*Pilkey*, 2014]. These data are processed with a time-of-arrival algorithm in order to find a series of 3-D points that represent the locations of VHF radio sources. The goodness of it for each LMA source is calculated via a reduced chi-square value. All the LMA data presented in this paper have been filtered to only include LMA sources that were detected by six or more stations and have a reduced chi-square value equal to or less than 5.

Figure 12 shows the LMA data during the UPL of UF 14-54 viewed from the south. Each dot represents an LMA source, and the color of the dot represents the power of each LMA source. The UPL branched at a relatively low altitude, 750 m, into a left-hand and a right-hand branch. A number of the LMA sources at the top of the right-hand branch have higher power than most of the other sources. Figure 13 shows the same LMA points as Figure 12 as a function of time, with $t = 0$ being the time of the TGF. Figure 13a shows LMA source power versus time, and Figure 13b shows LMA source altitude versus time. The green bars show the estimated start and stop times of the TGF. Figures 12 and 13 together show that the right-hand branch of the upward positive leader (UPL) was at an altitude of about 3.5 km during the time of the TGF and that the higher-power LMA sources occurred simultaneously with the TGF. The higher-power LMA sources occurred throughout the time of the TGF as opposed to being grouped together at the beginning or the end, with a few of the higher-power LMA points occurring after the end of the TGF.

High Speed Video Frames during ICC-pulse
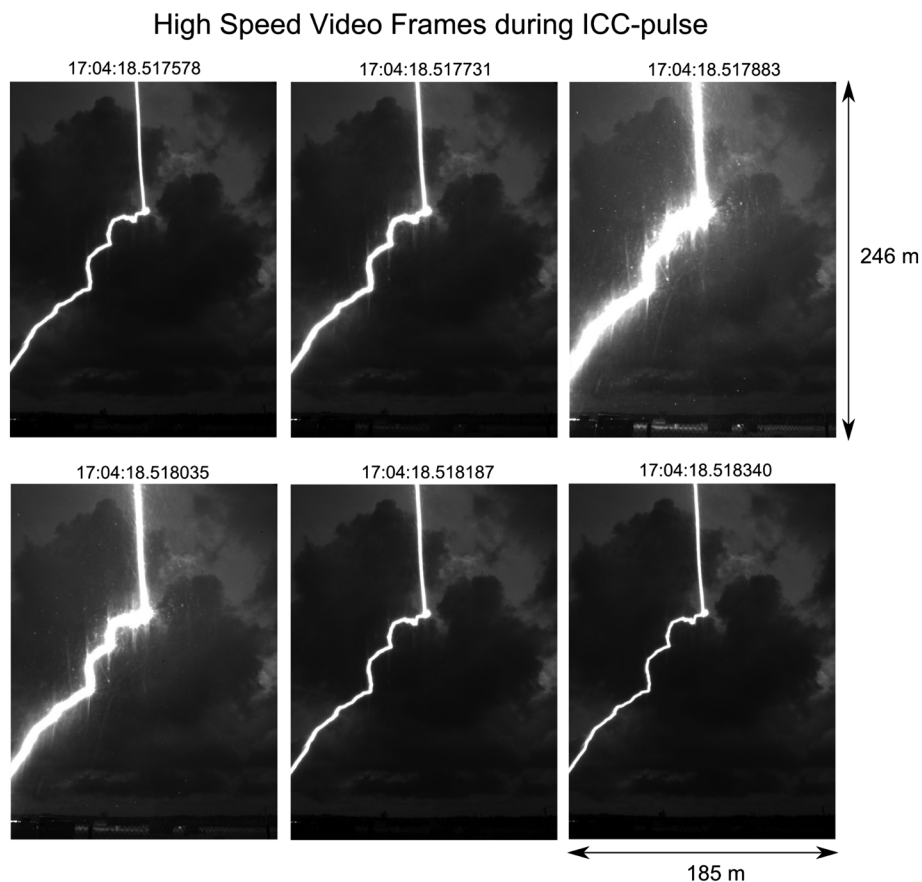
Figure 10. Pictured are six high-speed video frames of ICC pulse luminosity along and below the wire segment. The numbers above each frame indicate the UTC time stamp at the start of that frame. The high-speed camera had a frame rate of 6.5 kfps.
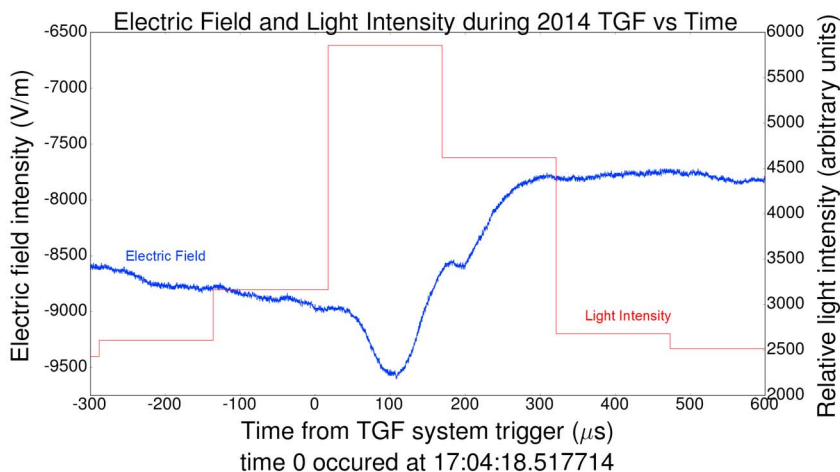
Figure 11. Electric field measured 105 m from the launcher and 150 m from the ground strike point by antenna E-NW100 and relative light intensity recorded during the 2014 TGF. This electric field was measured with a flat-plate antenna that is not sensitive to the quasi-static electric field, so the zero level, DC offset, of the electric field in this figure is arbitrary.
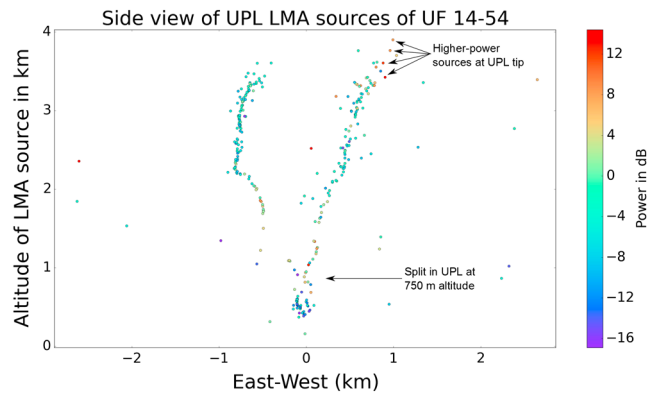
Figure 12. A side view of the UPL Lightning Mapping Array sources during UF 14-54, the flash that triggered the 2014 TGF. The figure shows a view looking at the UPL from the south. Note that this figure contains the same data points as Figure 13, both showing the LMA points from 20 ms before to about 15 ms after the TGF.

Figure 14 shows the LMA data for the entire UF 14-54 flash. Figure 14a shows the altitude of the LMA sources versus time. Figure 14b shows the altitude of the LMA sources versus east-west direction (left). Figures 14c and 14d show a plan view of the LMA sources (left) and a north-south direction versus altitude plot of the LMA sources (right). Figure 14e shows the distribution of LMA sources versus altitude. The left-hand branch of the UPL ceases to propagate at about 3.5 km altitude, but 88 ms after the TGF we associate with the right-hand branch, the left-hand branch initiates a leader that bifurcates around the location of the right-hand branch so that one section propagated north of the right-hand UPL and another section propagated south of the right-hand UPL, as indicated by black lines in Figure 14. Since this leader was an extension of the top of the left-hand UPL, it was positively charged, which indicates that there was still negative charge in the region near 3.5 km altitude, within a vertical kilometer or so after the TGF. After the TGF, the right-hand branch of the UPL was more active than the left branch and propagated up and into the main negative charge region of the storm near 5 km altitude.

Figure 15 shows LMA data from the UPL of UF 14-53, the classically triggered flash that was triggered about 7 min prior to the altitude-triggered flash UF 14-54. The UPL of UF 14-53 subdivides into a number of small branches starting around 2.5 km altitude before continuing to propagate into the cloud. Since it is known that UPLs and leaders in general tend to branch and to turn horizontal in regions of charge [*Hill et al.*, 2013; *Pilkey et al.*, 2014; *Coleman et al.*, 2003], the observation of branching suggests that there was negative charge at about 2.5 km to 3 km in altitude 7 min before the UF 14-54 TGF.
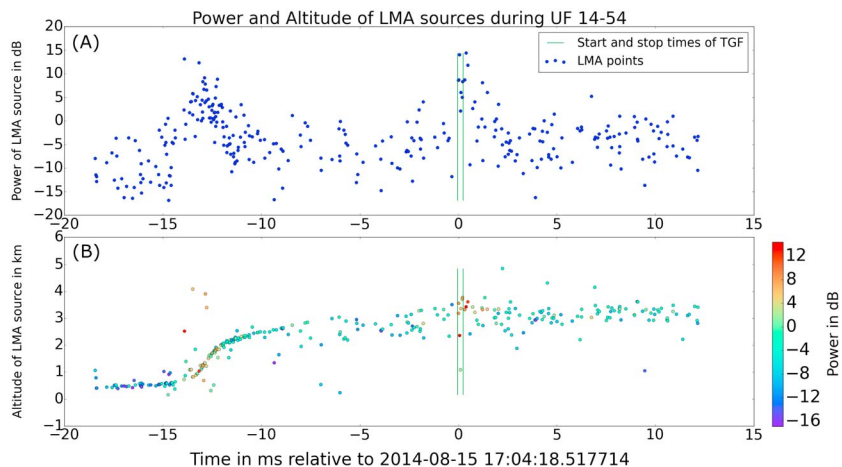
Figure 13. Power and altitude of Lightning Mapping Array sources during UF 14-54, the flash that triggered the 2014 TGF.
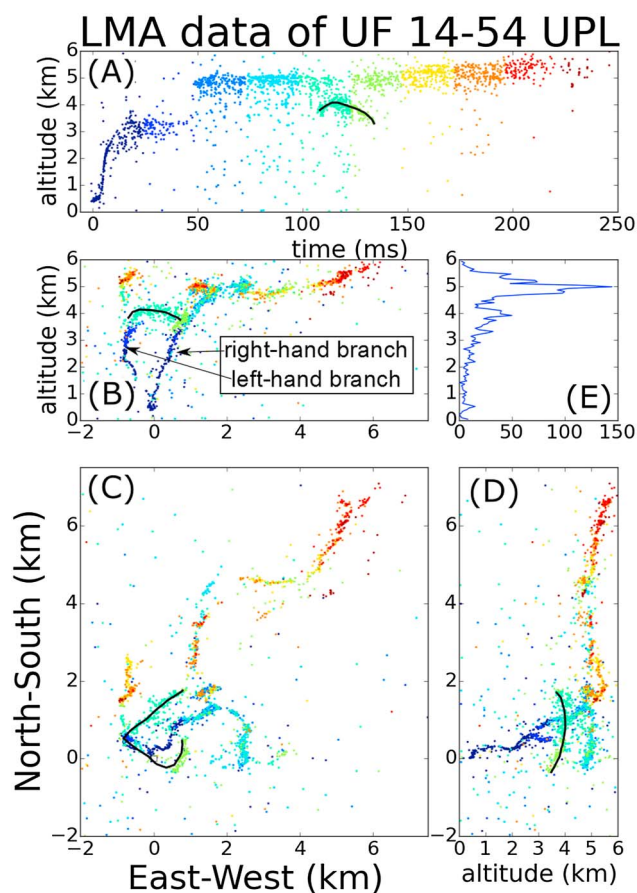
Figure 14. Lightning Mapping Array data of UF 14-54. (a) The altitude of the LMA sources versus time. (b) The altitude of the LMA sources versus east-west direction and (e) a histogram of number of LMA points versus altitude. (c) A plan view of the LMA sources and (d) a north-south direction versus altitude plot of the LMA sources. The black lines indicate an interesting propagating branched channel that starts near the top of the left UPL and propagates toward the right UPL 88 ms after the TGF. The two branches are clearly seen in the plan view but are at the same altitude and so cannot be distinguished in the side views.

3.5. Quasi-Static Electric Fields

Figure 16 shows the quasi-static electric fields, with the physics sign convention (a positive electric field at ground is produced by negative charge overhead), measured with a Campbell Scientific 110 electric field mill during the entire storm of 15 August 2014. The Campbell mills have DC response and sample the ambient field at 5 samples per second. In the ICLRT network there were eight such field mills. In Figure 16, both triggered flashes of 15 August 2014 are identified and are near the end of the storm, 7 min apart. Between the field changes due to the two triggered flashes there is a decrease in the electric field followed by an increase, indicating that some charge was moved or generated during this 7 min period. Possibilities for this charge distribution change could be a decreasing, or a rising, negative charge (or an increasing, or a falling, positive charge) overhead followed by an increasing, or a falling, negative charge (or a decreasing, or a rising, positive charge) overhead. The radar data presented next suggest that the decreasing portion of the electric field could potentially correspond to the growth of wet hydrometers around the freezing level of the storm, and the rising portion of the electric field likely corresponds to negative charge raining out of the cloud, as further discussed in section 3.6.

3.6. Radar

During summers 2011 through 2014, University of Oklahoma (OU) researchers operated a dual-polarimetric C band Shared Mobile Atmospheric Research and Teaching (SMART) radar [*Biggerstaff et al.*, 2005] located 12 km south of the ICLRT. It radiated at 5570 MHz in simultaneous transmit and receive mode with about 150 kW of peak power through each polarization channel. The radar had a half power beam width of 1.5°. During the
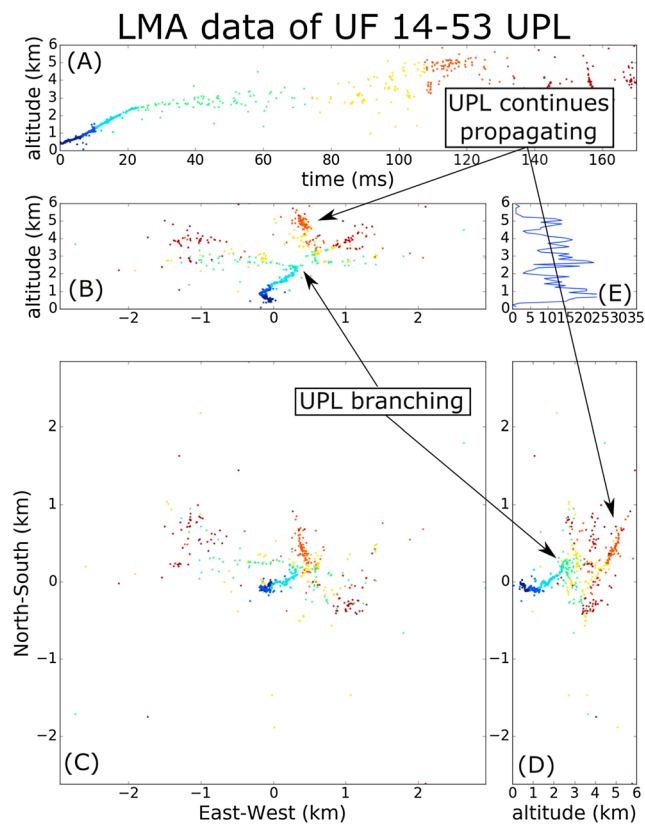
Figure 15. Lightning Mapping Array data of the UPL of UF 14-53 that was triggered 7 min prior to the TGF flash UF 14-54, showing where the UPL of UF 14-53 branched, which is near the same location that the UF 14-54 UPL that initiated a TGF 7 min later. UPL branching is thought to indicate a region of negative charge. (a) The altitude of the LMA sources versus time. (b) The altitude of the LMA sources versus east-west direction and (e) a histogram of number of LMA points versus altitude. (c) A plan view of the LMA sources and (d) a north-south direction versus altitude plot of the LMA sources.

15 August 2014 storm, the radar scanned every 17 s over ICLRT using range-height indicator (RHI) sweeps from 0° to 60° elevation.

Figure 17 shows the radar reflectivity data during UF 14-54 with a limited set of LMA source locations (black plus signs) of UF 14-54 overlaid. The LMA sources shown in Figures 17 and 18 include only LMA sources that are within 1 km of the plane of the radar echo. The radar site is at the origin of the plot. The white dot at 3.5 km altitude and a range of 13 km indicates the location of the high-power LMA sources associated with the TGF (Figures 12–14). To the left (south) and at higher altitudes with respect to the high-power LMA sources, an elevated maximum in radar reflectivity was observed straddling the freezing level. Farther north, this elevated precipitation core connected to the main dissipating convective rain shaft that extended down to the surface. This elevated reflectivity is in a hook-like shape, which indicates that there was a strong updraft that pushed the precipitation upward into the hook shape.

The storm of 15 August 2014 had a developing, a mature, and a dissipating stage similar to the conceptual model of weak-shear (air mass) multicell thunderstorms developed by *Byers and Braham* [1949], where the dissipating stage is characterized by precipitation-driven downdrafts from middle-to-low levels and weak residual updrafts aloft. The storm, however, had a late vigorous updraft during its dissipating stage. This updraft produced the precipitation that caused the elevated reflectivity core observed straddling the freezing level at the time of UF 14-54 that was discussed in the previous paragraph. Strong updrafts during the otherwise dissipating stages of multicell thunderstorms were rarely observed by the OU radar during the ~150 (2011 through 2014) days that was used to study Florida summertime convection. Perhaps the unusual vigorous updraft near the end of the storm was somehow related to precipitation charging associated with producing the TGF.
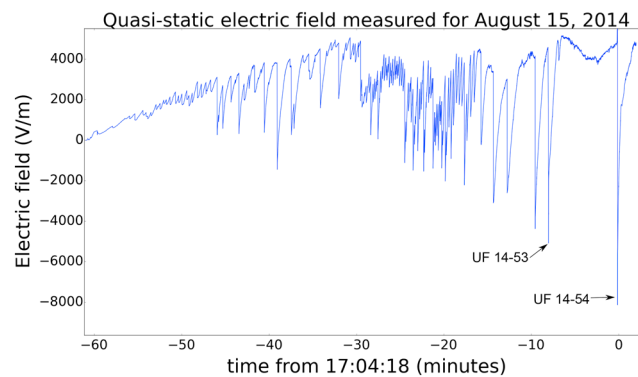
Figure 16. Quasi-static electric field measured on ground on 15 August 2014. Both triggered lightning flashes, UF 14-53 and UF 14-54, are labeled. The electric field is in the physics sign convention where negative charge overhead produces a positive electric field. Note the field change in the 7 min between UF 14-53 and UF 14-54, which could be interpreted as first a decreasing negative charge (or increasing positive charge) overhead followed by an increasing negative charge (or decreasing positive charge) overhead. Options are discussed in sections 3.5 and 3.6.

Specific differential phase (KDP), shown in Figure 18, is the range derivative of the backscatter phase difference between horizontal and vertical polarization channels from the OU dual-polarimetric radar. KDP measured by the OU radar at the time of the TGF showed strong positive values within the elevated core, including the portion of the core that extended above the freezing level, shown in Figure 18 with the upper left black arrow. Strongly positive KDP regions are associated with oblate raindrops or oblate hydrometeors with a thick shell of liquid water. Indeed, the main rain shaft (lower right black arrow in Figure 18) is also characterized by high values of KDP.

Since the elevated core was comprised of liquid or thickly water-coated hydrometeors, it is likely that any collisions with preexisting or in situ generated cloud ice would result in capture of the ice particles. Hence, rebounding ice particles were likely rare in the elevated reflectivity maxima. Given that the primary charging mechanism in convective clouds is thought to be the charge separation from rebounding ice-graupel collisions in the presence of supercooled water [*Takahashi*, 1978; *Saunders et al.*, 1991, 2006], the elevated reflectivity core was likely a region of weak charge. It is also possible that any charge that was separated resulted in net positive charge on the higher-density particles that remained near the freezing level since there was high liquid water content [*Saunders et al.*, 1991]. This is consistent with LMA data, shown in Figures 12, 14, and 17, that show that no positive lightning leaders from this flash extended into the elevated reflectivity core.

The decreasing portion of the ground-level quasi-static electric fields after UF 14-53, shown in Figure 16, is consistent with the growth of the wet, elevated reflectivity core displacing or neutralizing the preexisting negative charge or producing an area of weakly positive charge. The later increase in electric field, showing
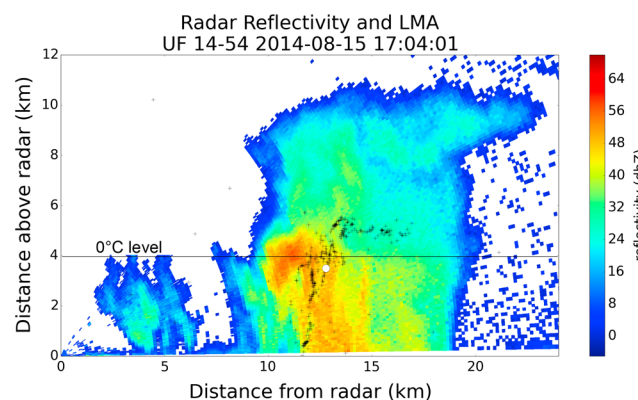
Figure 17. Range-height indicator (RHI) radar scan during UF 14-54 shows radar reflectivity. North is to the right. The black dots are LMA source locations showing the shape of UF 14-54. The radar site is at the origin of the plot and the ICLRT is 12 km north at the spot where the LMA sources from the UPL appear near ground level. The white dot at 3.5 km altitude indicates the location of the high-power LMA sources associated with the TGF.
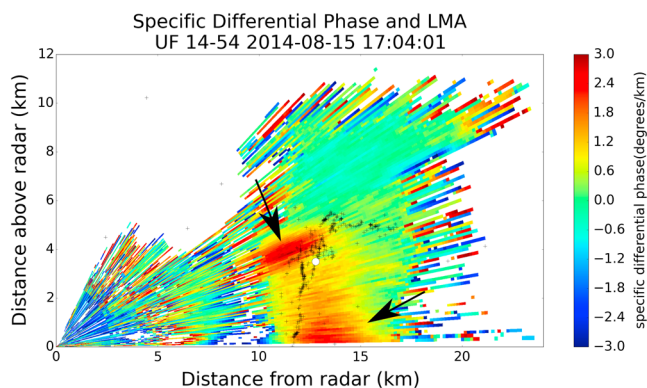
Figure 18. RHI radar scan during UF 14-54 shows radar specific differential phase (KDP). North is to the right. The radar site is at the origin of the plot and the ICLRT is 12 km north. The two black arrows show two interesting regions of high KDP. The upper arrow shows the high-reflectivity radar feature discussed in the text with a high KDP. The lower arrow points to a falling "packet" of high KDP, perhaps 3 km wide, that starts around the same time as the minimum of the static electric field shown in Figure 16 and reaches ground around the same time as UF 14-54 is triggered.

more net negative charge aloft, may be due to the descending nature of the main rain shaft. The lower region of high KDP, shown by the lower right arrow in Figure 18, started descending at about the same time as the minimum in static electric field between the two triggered flashes and reached the ground about the same time UF 14-54 was triggered. If the rain shaft contained net negative charge, it would explain the rising portion of the electric field just before UF 14-54.

3.7. Distant Magnetic Fields

Figure 19 shows measured magnetic fields from the TGF/ICC pulse recorded by three independent systems at a distance of about 250 km from the ICLRT, along with the modeled field to be discussed in section 4.

The University of Florida (UF) operates a single-loop VLF magnetic field antenna system in Melbourne, FL (28.06 N°, 80.62° W), about 250 km south of the ICLRT. This magnetic field receiver consists of an air-core loop antenna oriented to maximize the sensitivity to lightning flashes at the ICLRT, a preamplifier line receiver pair, and a computer-based sampling unit driven with GPS timing (100 ns absolute timing accuracy). The system is sensitive to frequencies between 3 and 47 kHz, and the data are sampled at 100 kHz with 16 bit resolution. System amplitude and phase calibration is performed by injecting known signal waveforms at the antenna and measuring the resulting output signals. The magnetic field antenna is located on the roof of the physics
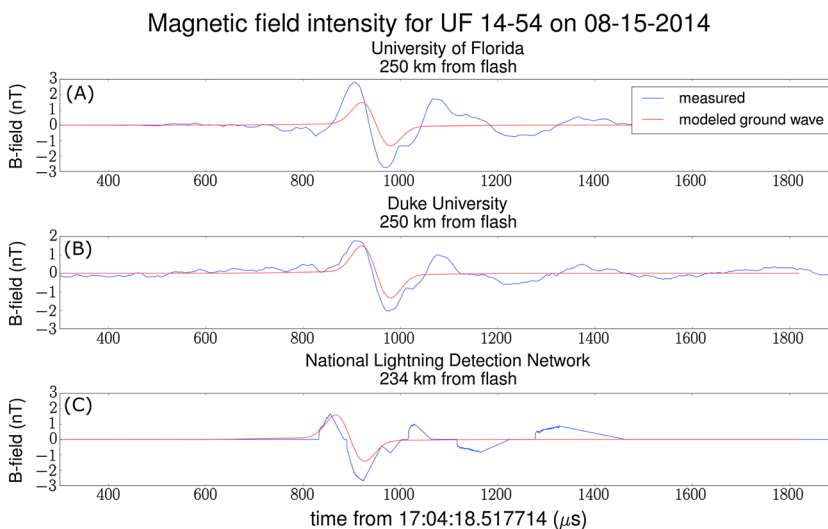
Figure 19. Measured (blue) and modeled (red) magnetic fields about 250 km from the ICLRT. The model does not include ionospheric reflections, only the ground wave, and so does not match any of the measured waveforms after the first cycle (the ground wave) when those ionospheric reflections arrive.

building at the Florida Institute of Technology (FIT), and no effort is made to account for any magnetic field enhancement or reduction caused by that structure. The UF VLF data for the TGF/ICC pulse are shown in Figure 19a.

Duke University operates a dual ferrite-core magnetic loop antenna system [*Cummer et al.*, 2011] on another part of the roof of the FIT physics building and measures the vector horizontal magnetic field at a sampling rate of 1 MHz with GPS-based timing. Data from this system presented here are postprocessed to have a flat frequency response between 1 kHz to 80 kHz and a single-pole response below 1 kHz. Amplitude calibration is achieved by comparison with a calibrated measurement on the ground in the vicinity of Duke University in North Carolina. The Duke University data are shown in Figure 19b.

The U.S. National Lightning Detection Network (NLDN) interpreted the ICC/TGF pulse as a 14.2 kA intracloud waveform. The NLDN magnetic field waveform, shown in Figure 19c, was measured by a sensor located close to Tampa, Florida, 234 km southwest of the ICLRT. Each NLDN sensor has an upper limit of frequency bandwidth of about 400 kHz and samples lightning magnetic field waveforms at a variable sampling rate above the sensor threshold so that all the waveform details and parameters relevant for geolocation, lightning type classification, and other applications are retained in the waveforms [*Cummins et al.*, 2012; *Honma et al.*, 2013]. Fine structure of lightning waveforms are retained for the initial rising portions of pulses (up to the initial peak or up to the last significant peak of the same polarity following the initial peak). Fine waveform features occurring after this are not necessarily retained unless their amplitudes are a significant fraction of the peak value. Also, data between the zero crossing of one polarity and sensor threshold of the opposite polarity are not measured. The result of this type of processing is evident in Figure 19c. The NLDN measures calibrated electromagnetic fields from individual lightning events at multiple locations and deduces currents from the field measurements via both a return-stroke model and a comparison with previous directly measured return-stroke currents in triggered lightning at the ICLRT.

4. Modeling

4.1. The 2013 UPL Line Charge Density Model

A model, similar to the model in *Pilkey* [2014], was used to analyze the line charge density of the upward positive leader (UPL) of the 2003 triggered flash that produced the TGF discussed in section 2. The model requires the UPL current as an input. The UPL current was directly measured in 2003 but could not be directly measured for the flash associated with the 2014 TGF because the altitude-triggered flash did not terminate on the launch structure which housed the current measurement. The model assumes that all the charge that enters the UPL at the bottom of the channel is deposited directly at the top of the channel. If we know the height of the top of the UPL at some time t, $z(t)$, then we can find the line charge density of the UPL between two points, $z(t)$ and $z(t + \triangle t)$, by integrating over the channel-base current from t to $t + \triangle t$ and dividing by the length $z(t + \triangle t) - z(t)$. Although we were only able to apply the model to the 2003 TGF, we would expect the derived line charge density for the 2014 case not to be much different since the TGF electric fields in 2003 and 2014 are similar, and the model-inferred channel-base current of 2014 (section 4.2) and the 2003 directly measured current are also similar.

Figure 20 shows the modeled line charge density for the UPL that initiated the 2003 TGF. Since there were no LMA data in 2003, the velocity of the UPL tip propagation could not be measured directly. Instead, the velocity of the UPL tip was chosen to be 1.1×10^5 m/s so that the modeled electric field at ground from the derived line charge density would approximate the measured electric field at ground. The 2003 electric field at ground was measured by a flat-plate antenna with 1 s decay time constant. LMA data show that the 2014 UPL had a maximum velocity of about 8×10^5 m/s from about 750 m altitude to 2 km altitude. After passing 2 km altitude, the UPL slowed down, and around 3.5 km altitude it had a velocity of about 1.5×10^5 m/s. Figure 21 shows the measured and modeled electric field during the 2003 UPL, illustrating that the model line charge density versus altitude produces a reasonable fit to the measured electric field at ground. Significantly, the derived line charge density is an order of magnitude larger than for a typical UPL [*Pilkey*, 2014], and we surmise that it was also the case for the 2014 UPL. More discussion is found in section 5.

4.2. The 2003 and 2014 ICC Pulse Model

In order to model the relationship between the close and distant electric fields at ground level and the currents of the ICC pulses for the 2003 and 2014 events, we use a modification of the M component model developed by *Rakov et al.* [1995], where the ICC pulse is viewed as a current wave that travels down the lightning channel
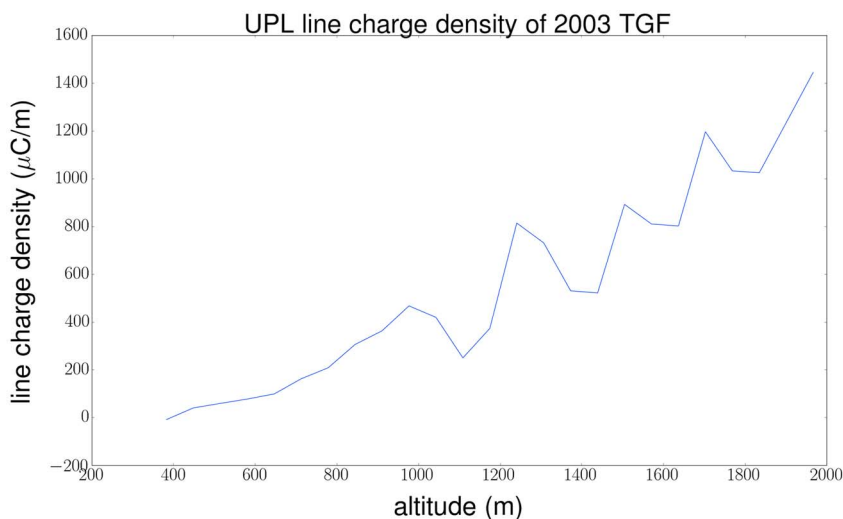
Figure 20. Line charge density of the UPL of UF 03-50, the rocket-triggered flash that initiated the 2003 TGF.

(assumed to be vertical above the rocket launcher) at a constant velocity with no attenuation or distortion. When this wave reaches the bottom of the channel, a large fraction of the current reflects and travels back up the channel at the same velocity. The model represents the simplest possible approach to providing a reasonable match to the measured electric field. In the model, the current on the lightning channel is described by equation (1) below, where $I(t,z)$ is the current at time t and altitude z on the channel, Γ is the current reflection coefficient at ground, I_g is the current measured at ground, and v is the velocity of the ICC current pulse on the channel. In equation (1), time t is defined to be 0 when the downward current wave first reaches the ground. Γ and v are the two pertinent parameters of this model, which are chosen to best fit the measured electric field.

$$I(t,z) = \begin{cases} \frac{1}{\Gamma+1} \times I_g(t+z/v) & : t < 0 \\ \frac{1}{\Gamma+1} \times I_g(t+z/v) + \frac{\Gamma}{\Gamma+1} \times I_g(t-z/v) & : t \geq 0. \end{cases} \quad (1)$$

The $\frac{1}{\Gamma+1}$ factor in the downward wave component in equation (1) is necessary because the channel-base current, I_g, is taken to be the known (measured) quantity. If the reflection coefficient changes, then the downward wave amplitude must change accordingly to keep the total (downward plus reflected) channel-base current unchanged. We can calculate the vertical electric fields at ground by inserting our current from equation (1), into equation (2) [*Uman et al.*, 1975], where H is the height of the channel, D is the horizontal distance from the channel to the measurement, c is the speed of light, R is the distance from the antenna to a channel segment
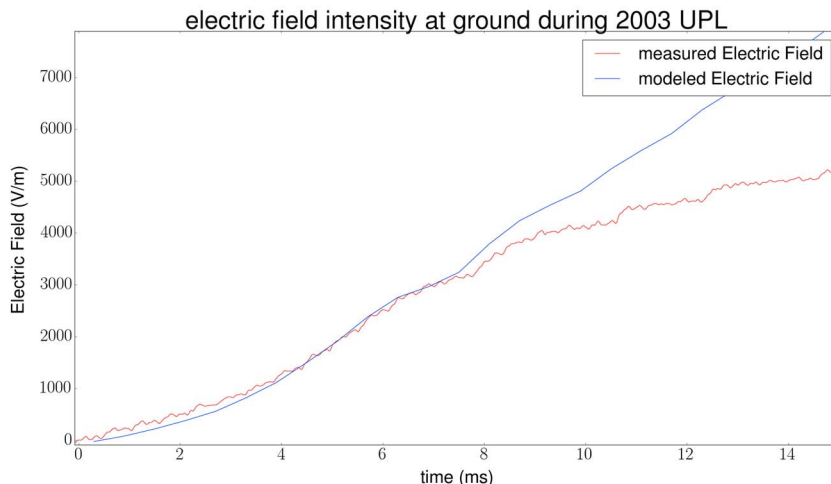
Figure 21. The measured (at ground) (red) and modeled (blue) electric field of the UF 03-50 UPL.
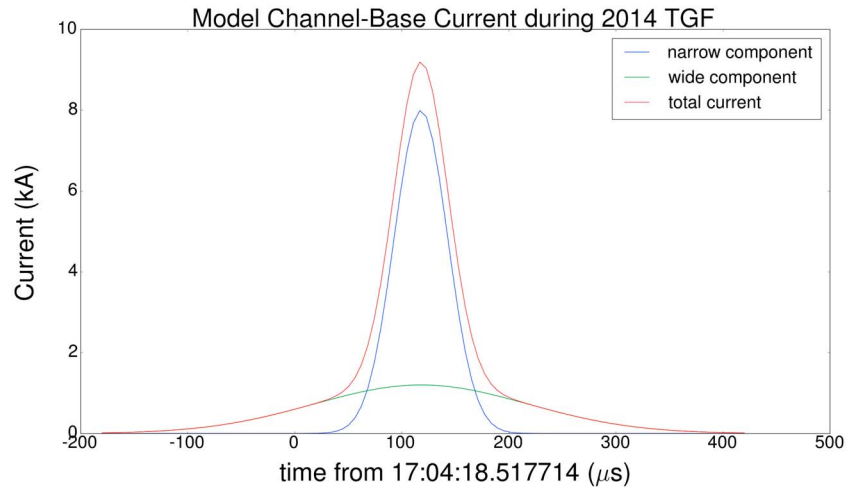
Figure 22. Channel-base current used in modeling the 2014 ICC pulse. The current is assumed to be a sum of two Gaussian functions. The rapidly varying Gaussian has an amplitude of 8 kA and a FWHM of 59 μs. The slowly varying Gaussian has an amplitude of 1.2 kA and a FWHM of 235 μs.

dz at height z, and θ is the angle between R and the vertical axis [see *Uman et al.*, 1975, Figure 2]. The three terms in equation (2) are called the electrostatic, induction, and radiation components, respectively. For distances in the 100 km range and for lightning impulsive waveforms, the radiation component will dominate the electrostatic and induction components. For distances less than 1 km both electrostatic and induction fields are significant and generally dominate the radiation fields. In the present work, we numerically calculate all three field components with no assumptions as to the relative significance of each field component. We also calculate the azimuthal component of the magnetic field using equation (3) [*Uman et al.*, 1975], which has two terms. The first term is called the induction field and the second is called the radiation field. The latter is dominant in our modeling of the ICC fields at 250 km. At that distance, the radiation fields of equations (2) and (3) are essentially proportional, and hence, $E_z = cB_\phi$.

$$E_z(D,t) = \frac{1}{2\pi\epsilon_0}\left[\int_0^H \frac{2-3\sin^2\theta}{R^3}\times\int_0^t I\left(z,\tau-\frac{R}{c}\right)d\tau dz + \int_0^H \frac{2-3\sin^2\theta}{cR^2}I(z,t-R/c)dz \right.$$
$$\left. -\int_0^H \frac{\sin^2\theta}{c^2R}\frac{\partial I(z,t-R/c)}{\partial t}dz\right] \qquad (2)$$

$$B_\phi(D,t) = \frac{\mu_0}{2\pi}\left[\int_0^H \frac{\sin\theta}{R^2}I(z,t-R/c)dz + \int_0^H \frac{\sin\theta}{cR}\frac{\partial I(z,t-R/c)}{\partial t}dz\right]. \qquad (3)$$

We first apply the model described above to the ICC pulse that occurred during the 2003 TGF. Figure 4 shows the results of equation (2) when the velocity of the ICC pulse in equation (1) is chosen to be 1.5×10^8 m/s and current reflection coefficient at ground is chosen to be 0.8. The $t = 0$ in Figure 4 matches with the $t = 0$ in equation (1). The match between the measured and modeled field is satisfactory.

Figure 9 shows the measured and modeled electric fields during the time of the 2014 ICC pulse and TGF for the same model, with the velocity and reflection coefficient parameters chosen to match the measured electric field. The 2014 best fit velocity and reflection coefficient have the same values that provide a best fit to the 2003 data, although in both cases the best fits are not perfect fits. Since channel-base current was not measured for the 2014 event, it was assumed that the channel-base current had the same wave shape as the channel-base current from 2003 in that it consisted of a rapidly varying Gaussian and a slowly varying Gaussian. This creates four extra parameters for the channel-base current, width and amplitude of the slowly and rapidly varying Gaussians, in producing the modeled electric field. The rapidly varying Gaussian was adjusted to have an amplitude of 8.0 kA and a FWHM of 59 μs, and the slowly varying Gaussian an amplitude of 1.2 kA and a FWHM of 235 μs in order to match the measured electric field. The close electric fields in Figure 9 are dominated by the electrostatic and induction components as determined by a calculation using equation (2). Figure 22 shows a plot of the modeled 2014 channel-base current versus time. The $t = 0$ in

Figure 22 is not the same as $t = 0$ in equation (1). Instead, we choose $t = 0$ in equation (1) to occur 140 μs before the $t = 0$ in Figure 22 in order to accommodate the Gaussian function's infinitely long tail. Since the quasi-steady background ICC in the lightning channel does not impact our measured electric fields, it is not possible to tell how much steady current was flowing when the ICC pulse shown in Figure 22 occurred. As noted earlier, the steady underlying current in 2003 was 1.3 kA.

Figure 19 shows the model results for the distant fields, shown in red overlaid on three independent magnetic field measurements taken at 250 km, 250 km, and 234 km from the ICLRT. Clearly, the match is very good considering the simplicity of the model.

5. Analysis and Discussion

In both 2003 and 2014, a downward TGF occurred during the initial stage of a triggered lightning flash (the former a classical trigger, the latter an altitude trigger), while the UPL was ascending toward or into a region of negative charge. The 2014 LMA data (there were no 2003 LMA data) show that when the TGF occurred, the tip of the UPL was at about 3.5 km altitude and that the bottom of the main negative charge region was near 5 km altitude. It is impossible to determine the exact height of the UPL during the 2003 TGF, but it was estimated by *Dwyer et al.* [2004a] to be about 6 km based on the time of the TGF, the expected speed of the UPL, and an assumed vertical UPL. It seems extremely improbable that there just happened to be a TGF during a UPL in both of these cases. Thus, somehow, the UPLs must have triggered the TGFs. This is further supported by the fact that relatively higher-power LMA sources were observed at the tip of the 2014 UPL at the time of the TGF. Furthermore, multi-MeV photons were detected for both the 2003 and 2014 TGFs, strongly suggesting that RREA was taking place during both events. This is in contrast with the alternative hypothesis that the TGFs were produced solely by cold runaway [*Carlson et al.*, 2010], which has been generally thought to produce X-rays, typically with energies below 1 MeV, at the tips of negative lightning leaders [*Dwyer et al.*, 2004b]. We know that Relativistic Runaway Electron Avalanches require large electric fields and high-energy seed particles [*Gurevich et al.*, 1992; *Dwyer*, 2012]. Thus, it seems most likely that in both 2003 and 2014, as the UPL traveled upward, it somehow triggered multiple downward RREAs over a period on the order of 100 μs that both emitted TGFs and delivered charge to the top of the UPL that traveled down the UPL as an ICC pulse. These RREAs had to be downward directed because the electric field above the UPL was upward in order to allow for propagation of the UPL, as supported by the ground-level measurements of the quasi-static electric field shown in Figure 16.

Twenty five to 30 UPLs have been triggered every summer since the TERA network was installed 10 years ago, but only the two UPLs discussed here have produced TGFs detected at the ICLRT. It is possible that there have been small TGFs that were not significant enough to be detected by the ICLRT. For example, UF 14-53, the triggered lightning flash 7 min before the TGF, had 43 counts (on the same unshielded NaI scintillator used in Figure 7) during its initial stage, which lasted 318 ms. However, with 95% statistical confidence, this count rate is well explained by the background rate of 136 counts per second. Future research will be needed to set similar limits for the other triggered flashes at the ICLRT. This, however, raises the question: what is special about these two UPLs? We know that the normal line charge density on an upward positive leader is on the order of hundreds of microcoulombs per meter [*Pilkey*, 2014]. Figure 20 shows that the modeled line charge density of the 2003 UPL was an order of magnitude larger than the usual value. Thus, the electric field aloft during the 2003 event must have been much larger than normal. While we could not determine the line charge density of the 2014 UPL, we know that altitude-triggered lightning requires relatively high ambient electric fields aloft because the electric field at the top of the elevated, isolated triggering wire is not enhanced as much as for a grounded wire. It is not known what is different between UF 14-54 and UF 14-53 that allowed UF 14-54 to initiate a detected TGF and not UF 14-53. Each rocket launch at the ICLRT initiates the triggering of all the scintillator measurements, in addition to the separate TGF-detection system that triggers the scintillators if there is a TGF occurring with or without the rocket launch trigger. For the case of UF 14-53, no statistically significant radiation was detected. The quasi-static electric field measurements and the radar measurements during the time between UF 14-53 and UF 14-54 strongly suggest that some negative charge aloft was being neutralized, or positive charge was being produced, that there was a descending rain shaft carrying negative charge, and that there was an unusual vigorous updraft that could have potentially contributed to UF 14-54 producing a TGF and UF 14-53 seemingly not doing so. Further investigation is required to determine if these meteorological phenomena were important, and if UF 14-53, and other UPLs at the ICLRT for that matter, could have produced TGFs that were not detected.

We know that RREA must have been present for the 2003 and 2014 events and that RREA requires a large electric field and a high-energy seed particle [*Gurevich et al.*, 1992]. However, because there could have been cold runaway [*Carlson et al.*, 2010; *Dwyer et al.*, 2004b] present associated with the UPL, along with the RREA, there are three possibilities for how the UPL triggered the RREA:

1. The seed particles for the RREA were primarily produced by cold runaway as the UPL passed through this region. The cold runaway could have been from streamers in front of the UPL or from a negative retrograde leader formed in a disconnected UPL branch [*Mazur and Ruhnke*, 2011; *Edens et al.*, 2012] as is often observed with negative stepped leaders and dart leaders near ground [*Dwyer et al.*, 2004b]. Note that the LMA does not show any evidence of a negative leader during or before the TGF, and negative leaders are most easily detected by the LMA, so if there was a negative leader, it would have had to be physically small and radiate weakly at VHF. In this scenario, the UPL would enhance the local electric field, but not enough for relativistic feedback (which will be the subject of scenario 3).

2. Cold runaway did not produce any significant number of seed particles, and the UPL did not enhance the electric field enough for relativistic feedback. In this case, the seed particles for the RREA would have to be due cosmic ray air showers passing through the region. This scenario seems unlikely, as relativistic feedback places a very strong limit on the strength of the electric field, and, thus, also places a strong limit on the avalanche multiplication of the RREA [*Dwyer*, 2003]. Thus, it seems unlikely that cosmic rays alone could provide a sufficient number of seed particles to produce a burst of gamma rays as intense as a TGF.

3. The UPL enhanced the local electric field enough to for relativistic feedback to occur, which then at least partially discharged the local electric field. This scenario is analogous to the model developed in *Dwyer* [2012].

The electric field/ICC pulse model provides a relatively good match to the close and distant measured fields in 2014, as shown in Figures 9 and 19. The model does not produce as good a match in 2003, but the model is still able to reproduce the major features of the measured waveform, as shown in Figure 4. Clearly, our model is not unique. It has been chosen to be the simplest possible model that can reproduce the significant features of the measured fields. It is certainly possible to formulate more complex models with different current characteristics and taking account of channel geometry that better match the observed electric fields. The present model does, however, provide two significant results. Since we were not able to record channel-base current during the 2014 TGF, we assumed the shape of the channel-base current measured in 2003. It is perhaps remarkable that the modeled electric field fits the measured electric field in 2014 so well with the assumed ICC pulse wave shapes. This very strongly suggests that the ICC current pulse in 2014 had both a slowly varying component and a more rapidly varying component, as in 2003, and that the respective components between 2003 and 2014 were approximately the same shape and amplitude.

Figure 23 shows the channel-base current used in modeling the 2014 ICC pulse along with the gamma radiation detected by a NaI scintillator where the travel time delays corresponding to a 3.5 km long channel have been removed from both the gamma radiation propagating at the speed of light (11.6 μs) and the model ICC pulse propagating at half the speed of light (23.3 μs). If there was no attenuation or distortion in the ICC pulse and the TGF as they traveled to ground, then Figure 23 shows the alignment of the two at the source, assuming their sources were both at the tip of the UPL at 3.5 km. In Figure 23, the more rapidly varying component of the channel current starts just after the TGF radiation begins. This supports our hypothesis that the rapidly varying component of the ICC current pulse is due to charge delivered to the top of the UPL channel by RREAs. However, since the optical transmission electronics (and possibly the PMT as well) for the gamma ray measurement used in Figure 23b became saturated, the time of the peak TGF flux might be different than what is shown in the figure. Proper modeling of the TGF may well confirm how well the ICC pulse current matches in time with the TGF flux at the source. We were not able to perform this analysis for the data collected from the 2003 TGF, since we do not know the location of the source of the 2003 TGF. However, Figure 2 shows that the peak of the ICC current pulse measured at the base of the channel occurred approximately 50 μs after the peak of the gamma ray flux. If the radiation source occurred at an altitude of 6 km with a perfectly vertical channel, and the current traveled half the speed of the gamma rays (as suggested by our modeling in section 4.2), then there would be a 20 μs difference between the peak of the gamma ray flux and the ICC pulse observed at the ground. The fact that the difference is 50 μs instead of 20 μs could easily be due to timing error, since, as noted in section 2, the scintillator data from 2003 could have exhibited a timing error where the gamma rays could have actually occurred up to 30 μs after the time shown in Figure 2. The 50 μs timing difference could also be due to the TGF source being at an altitude higher than 6 km, the channel turning horizontal and
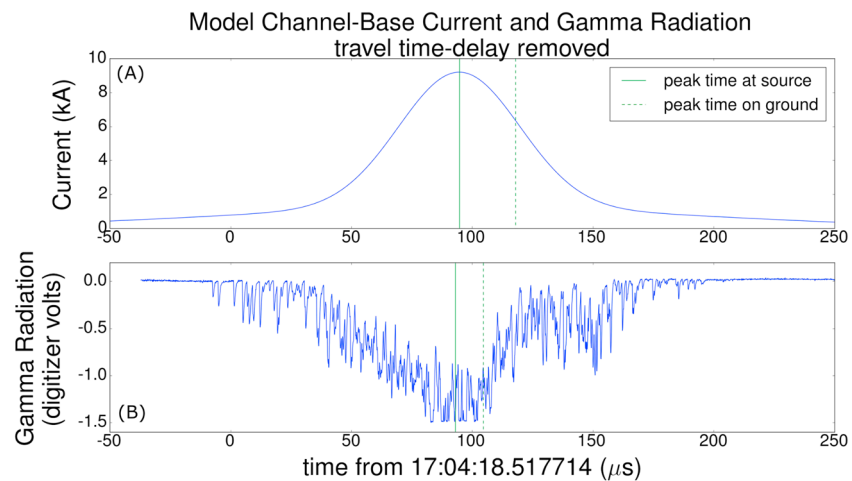
Figure 23. Same modeled current as shown in Figure 22 and gamma radiation shown in Figure 7 (but measured by a different NaI scintillator), except that time delays corresponding to a 3.5 km length channel were removed, with the current wave assumed propagating at 1.5×10^8 m/s and the gamma radiation propagating at the speed of light. The solid green vertical lines show the peak time of the two values at the source at 3.5 km altitude (that is, after the travel time was removed from the ground measurements), and dashed green vertical lines show peak time measured at ground. The time of TGF peak flux was found by looking at the gamma flux in this figure. However, since the fiber optic transmitter saturated near the time of peak flux, the actual time of the TGF peak flux may be slightly different than estimated.

being longer than 6 km when reaching the cloud's main charge region or the ICC pulse traveling slower than predicted by our model. From a physics standpoint, since the UPL is positively charged, the electrons in the RREA will accelerate toward the UPLs and it is physically reasonable that they could be collected by the UPL and then be conducted down the lightning channel. In both 2003 and 2014, the slowly varying component of the measured and modeled, respectively, channel-base current was observed to start long before the TGF (approximately 235 μs at the ground in 2003 and estimated 142 μs at the source in 2014). Thus, it is impossible that the RREA could have induced the slowly varying component of the current, and we conclude that it was likely the inherent UPL current increasing in response to a significantly increasing electric field with altitude.

The 2014 measured distant magnetic fields are essentially radiation field and are shown in Figure 19 along with the modeled magnetic fields. The magnetic fields measured by University of Florida, Duke University, and the NLDN are all very similar considering the differences in the measurement systems and their locations. The measurement made by the University of Florida is about a factor of 2 larger than that of Duke University and NLDN, but this could easily be due to magnetic field enhancement by the building on which the antenna is asymmetrically mounted. Our model produces a good fit to the first half cycles of the observed waveforms and a reasonable fit to the second half cycle. The measured data show that the second half cycle of the radiation fields have a larger amplitude than the first half cycle, which is not well modeled. Our model does not reproduce any of the cycles of the measured waveform following the first because our model does not take into account the ionospheric reflections that produce the signal after the first cycle and a half. We only model the so-called ground wave. We know from the modeling that the close electric fields shown in Figure 9 are composed of primarily electrostatic and induction components from current mainly in the lower portion of the ICC channel, while the distant electromagnetic fields shown in Figure 19 are purely radiation field from the ICC current in the whole path to 3.5 km altitude. The ability of our ICC pulse models to fit the close fields is relatively independent of its ability to fit the far fields, strengthening our confidence in the quality of the model.

The LMA data shown in Figure 15 indicate that there was negative charge near 2.5–3 km altitude 7 min prior to the 2014 TGF, and the LMA data in Figure 14 suggest that there was negative charge near 3.5–4 km altitude directly after the TGF. It is possible that the negative charge region that was at 2.5–3 km altitude 7 min before the TGF could have moved closer to 3.5–4 km altitude after the TGF. This relatively low-lying charge could have been the reason that the electric field aloft was high enough to create an altitude trigger, and this same charge could have induced the slowly varying component of the ICC pulse. These data suggest that a region of

negative charge created a relatively large electric field, which allowed the UPL to further enhance the ambient electric field sufficiently to create a TGF via RREA.

The 2003 and 2014 TGFs are similar to the several satellite-observed TGFs discussed by *Cummer et al.* [2014, 2015] in the sense that all were created by a charged leader approaching a charge region of opposite sign. However, our 2003 and 2014 TGFs differ from those discussed by *Cummer et al.* [2014, 2015] in that the latter TGFs were due to upward negatively charged leaders approaching positive charge regions and producing upward directed TGFs, while the ICLRT events were likely produced by upward positive leaders at 3.5 km and 6 km (for a vertical channel or lower otherwise) approaching negative charge. The three upward negative leaders tracked by *Cummer et al.* [2015] produced their TGFs in the middle of upward paths between roughly 8 km and 13 km. That is, the leaders continued to propagate upward after producing the TGFs, as does our 2014 UPL.

6. Summary

In this paper, we have described a Terrestrial Gamma Ray Flash observed at ground level in 2014 at the International Center for Lightning Research and Testing in North Central Florida. We have presented considerable data related to the TGF, including: close electric fields, high-speed optical records, LMA VHF locations, radar data, and three independent magnetic field waveforms recorded at about 250 km. We analyzed these data and compared them with data that were collected from a TGF in 2003, for which there was no radar or LMA data but channel-base current was directly measured. We found these two events to be very similar. Both TGFs occurred during the ascending stage of a UPL and had associated large ICC pulse in the channel to ground. LMA data suggest that in 2014, the TGF occurred from RREA near the tip of the UPL, as was likely the case in 2003. In both cases, there is no evidence of a negative leader before or during the TGF, so if there was a negative leader, it would have had to have been a weak retrograde negative leader (likely formed in a disconnected UPL branch), and the primary factor that triggered the TGF was the upward positive leader approaching a negative charge region. Modeling of the UPL line charge density in 2003 indicates that the thunderstorm in 2003 had unusually high electric fields aloft. Electric field/ICC pulse modeling suggests that the ICC current pulse during the 2014 TGF contained both a long-duration and a short-duration component, similar to the 2003 directly measured ICC pulse, and that the shorter duration component started about 50 µs after the RREA was initiated near the tip of the UPL, but this timing is imprecise as it relies upon simple modeling of the ICC pulse and a simplistic analysis of the scintillator data. The 2014 event produced distant (250 km) radiation fields that were relatively well reproduced by the same model used to successfully reproduce the close (100–200 m) fields, a downward propagating current wave that reflects off the ground.

References

Biggerstaff, M. I., L. J. Wicker, J. Guynes, C. Ziegler, J. M. Straka, E. N. Rasmussen, A. Doggett IV, L. D. Carey, J. L. Schroeder, and C. Weiss (2005), The shared mobile atmospheric research and teaching radar, *Bull. Am. Meteorol. Soc.*, *86*, 1263–1274.

Briggs, M. S., et al. (2010), First results on terrestrial gamma ray flashes from the Fermi Gamma-ray Burst Monitor, *J. Geophys. Res.*, *115*, A07322, doi:10.1029/2009JA015242.

Briggs, M. S., et al. (2011), Electron-positron beams from terrestrial lightning observed with Fermi GBM, *Geophys. Res. Lett.*, *38*, L02808, doi:10.1029/2010GL046259.

Byers, H. R., and R. R. Braham (1949), *The Thunderstorm*, 287 pp., U. S. Govt. Print. Off., Washington, D. C.

Chilingarian, A., A. Daryan, K. Arakelyan, A. Hovhannisyan, B. Mailyan, L. Melkumyan, G. hovsepyan, S. Chilingaryan, A. Reymers, and L Vanyan (2010), Ground-based observations of thunderstorm-correlated fluxed of high-energy electrons, gamma rays and neutrons, *Phys. Rev.*, *82*, 43009, doi:10.1103/PhysRevD.82.043009.

Carlson, B. E., N. G. Lehtinen, and U. S. Inan (2010), Terrestrial gamma ray flash production by active lightning leader channels, *J. Geophys. Res.*, *115*, A10324, doi:10.1029/2010JA015647.

Cohen, M. B., U. S. Inan, R. K. Said, M. S. Briggs, G. J. Fishman, V. Connaughton, and S. A. Cummer (2010), A lightning discharge producing a beam of relativistic electrons into space, *Geophys. Res. Lett.*, *37*, L18806, doi:10.1029/2010GL044481.

Coleman, L. M., T. C. Marshall, M. Stolzenburg, T. Hamlin, P. R. Krehbiel, W. Rison, and R. J. Thomas (2003), Effects of charge and electrostatic potential on lightning propagation, *J. Geophys. Res*, *108*(D9), 4298, doi:10.1029/2002JD0027181.

Connaughton, V., et al. (2010), Associations between Fermi Gamma-ray Burst Monitor terrestrial gamma ray flashes and sferics from the World Wide Lightning Location Network, *J. Geophys. Res.*, *115*, A12307, doi:10.1029/2010JA015681.

Connaughton, V., et al. (2013), Radio signals from electron beams in terrestrial gamma ray flashes, *J. Geophys. Res. Space Physics*, *118*, 2313–2320, doi:10.1029/2012JA018288.

Cummer, S. A., Y. Zhai, W. Hu, D. M. Smith, L. I. Lopez, and M. A. Stanley (2005), Measurements and implications of the relationship between lightning and terrestrial gamma ray flashes, *Geophys. Res. Lett.*, *32*, L08811, doi:10.1029/2005GL022778.

Cummer, S. A., G. Lu, M. S. Briggs, V. Connaughton, S. Xiong, G. J. Fishman, and J. R. Dwyer (2011), The lightning-TGF relationship on microsecond timescales, *Geophys. Res. Lett.*, *38*, L14810, doi:10.1029/2011GL048099.

Cummer, S. A., M. S. Briggs, J. R. Dwyer, X. Xiong, V. Connaughton, G. J. Fishman, G. Lu, F. Lyu, and R. Solanki (2014), The source altitude, electric current, and intrinsic brightness of terrestrial gamma ray flashes, *Geophys. Res. lett.*, *41*, 8586–8593, doi:10.1002/2014GL062196.

Cummer, S. A., F. Lyu, M. S. Briggs, G. Fitzpatrick, O. J. Roberts, and J. R. Dwyer (2015), Lightning leader altitude progression in terrestrial gamma-ray flashes, *Geophys. Res. Lett.*, *42*, 7792–7798, doi:10.1002/2015GL065228.

Cummins, K. L., N. Honma, A. E. Pifer, T. Rogers, and M. Tatsumi (2012), Improved detection of winter lightning in the Tohoku region of Japan using Vaisala's LS700x technology, *Inst. Electr. Eng. Jpn.*, *132*(6), 529–535, doi:10.1541/ieejpes.123.529.

Dwyer, J. R. (2003), A fundamental limit on electric fields in air, *Geophys. Res. Lett.*, *30*(20), 2055, doi:10.1029/2003GL017781.

Dwyer, J. R. (2012), The relativistic feedback discharge model of terrestrial gamma ray flashes, *J. Geophys. Res.*, *117*, A02308, doi:10.1029/2011JA017160.

Dwyer, J. R., and D. M. Smith (2005), A comparison between Monte Carlo simulations of runaway breakdown and terrestrial gamma-ray flash observations, *Geophys. Res. Lett.*, *32*, L22804, doi:10.1029/2005GL023848.

Dwyer, J. R., and M. A. Uman (2013), The physics of lightning, *Phys. Rep.*, *534*, 147–241, doi:10.1016/j.physrep.2013.09.004.

Dwyer, J. R., H. K. Rassoul, M. Al-Dayeh, L. Caraway, B. Wright, A. C. M. A. Uman, V. A. Rakov, K. J. Rambo, D. M. Jordan, J. Jerauld, and C. Smyth (2004a), A ground level gamma-ray burst observed in association with rocket-triggered lightning, *Geophys. Res. Lett.*, *31*, L05119, doi:10.1029/2003GL018771.

Dwyer, J. R., et al. (2004b), Measurements of X-ray emission from rocket-triggered lightning, *Geophys. Res. Lett.*, *31*, L05118, doi:10.1029/2003GL018770.

Dwyer, J. R., D. M. Smith, M. A. Uman, Z. Saleh, B. Grefenstette, B. Hazelton, and H. K. Rassoul (2010), Estimation of the fluence of high-energy electron bursts produced by thunderclouds and the resulting radiation doses received in aircraft, *J. Geophys. Res.*, *115*, D09206, doi:10.1029/2009JD012039.

Dwyer, J. R., M. M. Schaal, E. Cramer, S. Arabshahi, N. Liu, H. K. Rassoul, J. D. Hill, D. M. Jordan, and M. A. Uman (2012), Observation of a gamma-ray flash at ground level in association with a cloud-to-ground lightning return stroke, *J. Geophys. Res.*, *117*, A10303, doi:10.1029/2012JA017810.

Edens, H. E., et al. (2012), VHF lightning mapping observations of a triggered lightning flash, *Geophys. Res. Lett.*, *39*, L19807, doi:10.1029/2012GL053666.

Fishman, G. J., et al. (1994), Discovery of intense gamma-ray flashes of atmospheric origin, *Science*, *264*, 1313–1316, doi:10.1126/science.264.5163.1313.

Grefenstette, B. W., D. M. Smith, J. R. Dwyer, and G. J. Fishman (2008), Time evolution of terrestrial gamma ray flashes, *Geophys. Res. Lett.*, *35*, L06802, doi:10.1029/2007GL032922.

Gurevich, A. V., G. M. Milikh, and R. Roussel-Dupré (1992), Runaway electron mechanism of air breakdown and preconditioning during a thunderstorm, *Phys. Lett. A*, *165*, 463–468.

Hill, J. D., J. Pilkey, M. A. Uman, D. M. Jordan, W. Rison, and P. R. Krehbiel (2012), Geometrical and electrical characteristics of the initial stage in Florida triggered lightning, *Geophys. Res. Lett.*, *39*, L09807, doi:10.1029/2012GL051932.

Hill, J. D., J. Pilkey, M. A. Uman, D. M. Jordan, W. Rison, P. R. Krebhiel, M. I. Biggerstaff, P. Hyland, and R. Blakeslee (2013), Correlated lightning mapping array and radar observations of the initial stages of three sequentially triggered Florida lightning discharges, *J. Geophys. Res. Atmos.*, *118*, 8460–8481, doi:10.1002/jgrd.50660.

Honma, N., K. L. Cummins, M. J. Murphy, A. E. Pifer, and T. S. Rogers (2013), Improved lightning locations in the Tohoku Region of Japan using propagation and waveform onset corrections, *IEE J. Trans. Power Energy*, *133*(2), 195–202, doi:10.1541/ieejpes.133.195.

Inan, U. S., S. C. Reising, G. J. Fishman, and J. M. Horack (1996), On the association of terrestrial gamma-ray bursts with lightning and implication for sprites, *Geophys. Res. Lett.*, *23*(9), 1017–1020, doi:10.1029/96GL00746.

Lalande, P., A. Bondiou-Clergerie, P. Laroche, A. Eybert-Berard, J.-P. Berlandis, B. Bador, A. Bonamy, M. A. Uman, and V. A. Rakov (1998), Leader properties determined with triggered lightning techniques, *J. Geophys. Res.*, *103*, 14,109–14,115, doi:10.1029/97JD02492.

Lu, G., R. J. Blakeslee, J. Li, D. M. Smith, X.-M. Shao, E. W. McCaul, D. E. Buechler, H. J. Christian, J. M. Hall, and S. A. Cummer (2010), Lightning mapping observation of a terrestrial gamma-ray flash, *Geophys. Res. Lett.*, *37*, L11806, doi:10.1029/2010GL043494.

Marisaldi, M., et al. (2010), Detection of terrestrial gamma ray flashes up to 40 MeV by the AGILE satellite, *J. Geophys. Res.*, *115*, A00E13, doi:10.1029/2009JA014502.

Mazur, V., and L. H. Ruhnke (2011), Physical processes during development of upward leaders from tall structures, *J. Electrost.*, *69*, 97–110, doi:10.1016/j.elstat.2011.01.003.

McCarthy, M., and G. K. Parks (1985), Further observations of X-rays inside thunderstorms, *Geophys. Res. Lett.*, *12*(6), 393–396.

Østgaard, N., T. Gjesteland, B. E. Carlson, A. B. Collier, S. A. Cummer, G. Lu, and H. J. Christian (2013), Simultaneous observations of optical lightning and terrestrial gamma ray flash from space, *Geophys. Res. Lett.*, *40*, 2423–2426, doi:10.1002/grl.50466.

Pilkey, J. T., M. A. Uman, J. D. Hill, T. Ngin, W. R. Gamerota, D. M. Jordan, J. Caicedo, and B. Hare (2014), Rocket-triggered lightning propagation paths relative to preceding natural lightning activity and inferred cloud charge, *J. Geophys. Res. Atmos.*, *119*, 13,426–13,456, doi:10.1002/2014JD022139.

Pilkey, J. T. (2014), Rocket-triggered lightning propagation and North-Florida thunderstorm charge structure, Doctorate (PhD), Electr. Comput. Eng., Univ. of Florida, Gainesville, Fla. [Available at http://ufdc.ufl.edu/UFE0047331/ 00001.]

Rakov, V. A., R. Thottappillil, and M. A. Uman (1995), Mechanism of the lightning M component, *J. Geophys. Res.*, *100*, 25,701–25,710, doi:10.1029/95JD01924.

Rakov, V. A., and M. A. Uman (2003), *Lightning Physics and Effects*, Cambridge Univ. Press, Cambridge, U. K.

Saunders, C. P. R., W. D. Keith, and R. P. Mitzeva (1991), The effect of liquid water on thunderstorm charging, *J. Geophys. Res.*, *96*, 11,007–11,017.

Saunders, C. P. R., H. Bax-Norman, C. Emersic, E. E. Avila, and N. E. Castellano (2006), Laboratory studies of the effect of cloud conditions on graupel/crystal charge transfer in thunderstorm electrification, *Quart. J. R. Meteorol. Soc.*, *132*, 2653–2673.

Shao, X. M., T. Hamlin, and D. M. Smith (2010), A closer examination of terrestrial gamma-ray flash-related lightning processes, *J. Geophys. Res.*, *115*, A00E30, doi:10.1029/2009JA014835.

Smith, D. M., L. I. Lopez, R. P. Lin, and C. P. Barrington-Leigh (2005), Terrestrial gamma-ray flashes observed up to 20 MeV, *Science*, *307*, 1085–1088.

Takahashi, T. (1978), Riming electrification as a charge generation mechanism in thunderstorms, *J. Atmos. Sci.*, *35*, 1536–1548.

Tran, M. D., V. A. Rakov, S. Mallick, J. R. Dwyer, A. Nagc, and S. Heckman (2015), A terrestrial gamma-ray flash recorded at the Lightning Observatory in Gainesville, Florida, *J. Atmos. Sol. Terr. Phys.*, *136*, 86–93, doi:10.1016/j.jastp.2015.10.010.

Uman, M. A., D. K. McLain, and E. P. Krider (1975), Electromagnetic radiation from a finite antenna, *Am. J. Phys.*, *43*(1), 33–38.